Table III. Multivariate analysis of the results of treatment on hearing outcome (polytomous universal model).

Parameter	B	SEM	Wald	*p* value
Severity				
Moderate	–0.28	0.60	0.22	0.64
Severe	–0.11	0.50	0.05	0.82
Profound	0.00			
Hypercholesterolemia				
–	0.09	0.45	0.04	0.85
+	0.00			
Age group				
Young	–0.18	0.64	0.08	0.78
Middle-aged	0.69	0.49	1.97	0.16
Old	0.00			
Hyperglycemia				
–	–0.20	0.67	0.09	0.77
+	0.00			
Hypertension				
–	–0.26	0.52	0.24	0.62
+	0.00			
Vertigo				
–	–0.91	0.48	3.71	0.05
+	0.00			
Contralateral hearing loss				
–	–2.51	0.66	14.33	<0.001*
+	0.00			

The analysis of these treatment outcomes showed that a past history of contralateral hearing loss was significantly correlated with reduced recovery. B, regression coefficient; SEM, standard error of the mean; Wald, Wald statistics.
*$p < 0.01$.

they concluded that patients with previously diagnosed hearing loss in the opposite ear had poor hearing results [7] and the correlation between hearing recovery in the affected ear and hearing in the opposite ear was significant. In our study, similar to the study of Cvorović et al., we demonstrated poor hearing outcomes in ISSNHL patients with prior contralateral hearing loss. This discrepancy between studies may be explained by the patient selection criteria. In the present study we excluded those with low-frequency hearing loss in order to exclude patients with delayed endolymph hydrops. Patients with previous hearing loss often develop endolymph hydrops in the opposite ear (delayed endolymph hydrops), and short-term hearing recovery is good in such patients. Cvorović et al. included only a small number of patients with low-frequency hearing loss (4.7%) [7], whereas in the study by Stahl and Cohen, five of nine patients showed up-slope hearing loss and two patients experienced the recurrence of hearing loss [10], suggesting that these patients were affected by endolymph hydrops. These data could explain the more favorable hearing results reported in that study for patients with contralateral hearing loss.

Microvascular disease is one candidate for the pathophysiology of ISSNHL. Metabolic and circulatory diseases including hyperglycemia, hypercholesterolemia, and hypertension are well known risk factors for microvascular diseases. The levels of triglycerides, total cholesterol, and lipoprotein A are often significantly higher in patients with sudden deafness than in control subjects [11]. However, the influence of such metabolic diseases on the hearing outcomes of ISSNHL is still controversial. Orita et al. reported that ISSNHL patients with hyperglycemia and hypercholesterolemia had improved hearing results [5]. In the present study, however, we did not find that such diseases were correlated to the outcomes of ISSNHL. This discrepancy may be explained by the different treatment regimens employed. Orita et al. used prostaglandin and hyperbaric oxygen administration, which may be beneficial in patients with microvascular diseases [5]. Another study using a similar treatment regimen to ours reported that ISSNHL patients with hyperglycemia, hypercholesterolemia, and hypertension showed poor hearing results [12]. These results suggest that modification of the treatment regimen may be preferable in ISSNHL patients with risk factors for microvascular diseases.

Declaration of interest: This work was supported by Grants-in-aid for Young Scientists (B) from the Japan Society of the Promotion of Science 21791612. The authors report no conflicts of interest. The authors alone are responsible for the content and writing of the paper.

References

[1] Nakashima T, Tanabe T, Yanagita N, Wakai K, Ohno Y. Risk factors for sudden deafness: a case-control study. Auris Nasus Larynx 199;24:265–70.
[2] Veltri RW, Wilson WR, Sprinkle PM, Rodman SM, Kavesh DA. The implication of viruses in idiopathic sudden hearing loss: primary infection or reactivation of latent viruses? Otolaryngol Head Neck Surg 1981;89:137–41.
[3] Capaccio P, Ottaviani F, Cuccarini V, Bottero A, Schindler A, Cesana BM, et al. Genetic and acquired prothrombotic risk factors and sudden hearing loss. Laryngoscope 2007;117:547–51.
[4] Yeo SW, Park SN, Park YS, Suh BD, Han H, Choi HB, et al. Different distribution of HLA class II alleles according to response to corticosteroid therapy in sudden sensorineural hearing loss. Arch Otolaryngol Head Neck Surg 2001;127:945–9.

[5] Orita S, Fukushima K, Orita Y, Nishizaki K. Sudden hearing impairment combined with diabetes mellitus or hyperlipidemia. Eur Arch Otorhinolaryngol 2007;264:359–62.
[6] Weng SF, Chen YS, Hsu CJ, Tseng FY. Clinical features of sudden sensorineural hearing loss in diabetic patients. Laryngoscope 2005;115:1676–80.
[7] Cvorović L, Deric D, Probst R, Hegemann S. Prognostic model for predicting hearing recovery in idiopathic sudden sensorineural hearing loss. Otol Neurotol 2008;29: 464–9.
[8] Xenellis J, Karapatsas I, Papadimitriou N, Nikolopoulos T, Maragoudakis P, Tzagkaroulakis M, et al. Idiopathic sudden sensorineural hearing loss: prognostic factors. J Laryngol Otol 2006;120:718–24.
[9] Kanzaki J, Inoue Y, Ogawa K, Fukuda S, Fukushima K, Gyo K, et al. Effect of single-drug treatment on idiopathic sudden sensorineural hearing loss. Auris Nasus Larynx 2003; 30:123–7.
[10] Stahl N, Cohen D. Idiopathic sudden sensorineural hearing loss in the only hearing ear: patient characteristics and hearing outcome. Arch Otolaryngol Head Neck Surg 2006;132:193–5.
[11] Lu YY, Jin Z, Tong BS, Yang JM, Liu YH, Duan M. A clinical study of microcirculatory disturbance in Chinese patients with sudden deafness. Acta Otolaryngol 2008;128:1168–72.
[12] Hirano K, Ikeda K, Kawase T, Oshima T, Kekehata S, Takahashi S, et al. Prognosis of sudden deafness with special reference to risk factors of microvascular pathology. Auris Nasus Larynx 1999;26:111–15.

DOI: 10.3171/2010.2.JNS091817

Mechanical stress-induced reactive gliosis in the auditory nerve and cochlear nucleus

Laboratory investigation

Tetsuji Sekiya, M.D.,[1] Masahiro Matsumoto, M.D.,[1,2] Ken Kojima, M.D.,[1] Kazuya Ono, B.Pharm.,[1] Yayoi S. Kikkawa, M.D.,[1] Shinpei Kada, M.D.,[1] Hideaki Ogita, M.D.,[1] Rie T. Horie, M.D.,[1] Arpad Viola, M.D.,[3] Matthew C. Holley, Ph.D.,[4] and Juichi Ito, M.D.[1]

[1]Department of Otolaryngology, Head and Neck Surgery, Kyoto University Graduate School of Medicine, Kyoto, Japan; [2]Department of Otorhinolaryngology, University of Tübingen, Germany; [3]Department of Neurosurgery, St. John's Hospital, Budapest, Hungary; and [4]Department of Biomedical Science, The University of Sheffield, England

Object. Hearing levels following microsurgical treatment gradually deteriorate in a number of patients treated for vestibular schwannoma (VS), especially in the subacute postoperative stage. The cause of this late-onset deterioration of hearing is not completely understood. The aim of this study was to investigate the possibility that reactive gliosis is a contributory factor.

Methods. Mechanical damage to nerve tissue is a feature of complex surgical procedures. To explore this aspect of VS treatment, the authors compressed rat auditory nerves with 2 different degrees of injury while monitoring the compound action potentials of the auditory nerve and the auditory brainstem responses. In this experimental model, the axons of the auditory nerve were quantitatively and highly selectively damaged in the cerebellopontine angle without permanent compromise of the blood supply to the cochlea. The temporal bones were processed for immunohistochemical analysis at 1 week and at 8 weeks after compression.

Results. Reactive gliosis was induced not only in the auditory nerve but also in the cochlear nucleus following mechanical trauma in which the general shape of the auditory brainstem response was maintained. There was a substantial outgrowth of astrocytic processes from the transitional zone into the peripheral portion of the auditory nerve, leading to an invasion of dense gliotic tissue in the auditory nerve. The elongated astrocytic processes ran in parallel with the residual auditory neurons and entered much further into the cochlea. Confocal images disclosed fragments of neurons scattered in the gliotic tissue. In the cochlear nucleus, hypertrophic astrocytic processes were abundant around the soma of the neurons. The transverse diameter of the auditory nerve at and proximal to the compression site was considerably reduced, indicating atrophy, especially in rats in which the auditory nerve was profoundly compressed.

Conclusions. The authors found for the first time that mechanical stress to the auditory nerve causes substantial reactive gliosis in both the peripheral and central auditory pathways within 1–8 weeks. Progressive reactive gliosis following surgical stress may cause dysfunction in the auditory pathways and may be a primary cause of progressive hearing loss following microsurgical treatment for VS. *(DOI: 10.3171/2010.2.JNS091817)*

Key Words • **auditory nerve** • **auditory brainstem response** • **cochlear nucleus** • **hearing loss** • **reactive gliosis** • **vestibular schwannoma**

A growing body of evidence indicates that a significant number of patients with VS experience progressive hearing loss following microsurgical intervention. A controlled prospective study has not been performed, and the existing reports are characterized by substantial interpatient variation with respect to hearing level, definition of hearing preservation, and length of the follow-up period. However, hearing loss ranges from 15–40%, within mean follow-up periods of 5–9 years.[5,9,18,32,58,59] In one report as many as 56% of patients (14 of 25) had experienced a decline in hearing quality in the surgically treated ear 20 years after surgery, with only 1 patient experiencing a similar loss in the contralateral ear.[47] Although several explanations have been proposed,

Abbreviations used in this paper: ABR = auditory brainstem response; CAP = compound action potential; CPA = cerebellopontine angle; CR = compression-recording; EDTA = ethylenediaminetetraacetic acid; GFAP = glial fibrillary acidic protein; IAA = internal auditory artery; IAC = internal auditory canal; IAM = internal auditory meatus; IPL = interpeak latency; PBS = phosphate-buffered saline; PNS = peripheral nervous system; TSF = tractus spiralis foraminosus; TZ = transitional zone; VS = vestibular schwannoma.

This article contains some figures that are displayed in color online but in black and white in the print edition.

none has been demonstrated experimentally, and the primary cause remains unknown.

There are several potential causes of hearing loss following surgery. During surgery the contents of the IAC and the surrounding structures in the CPA are mechanically manipulated, which may cause axon degeneration and/or constriction of the arterial blood supply to the cochlea along with fibrosis and scarring in the CPA.[20,47] These reported pathological processes are likely to act together with a combinatorial effect.

Reactive gliosis has not been proposed as a cause, but it is often associated with trauma to the CNS, including that caused by ischemia, radiation, genetic disorders, or chemical insult.[6,13,21,38] A considerable number of quiescent astrocytes can resume proliferation, become hypertrophic, and upregulate GFAP.[19,28,39,52,56]

The mechanical effects of surgery are complex but can be broken down in terms of various forces, such as stretching, laceration, and compression.[7] Evaluating the effects of compression is thus clinically relevant. In this report, we demonstrate for the first time that mechanical compression applied to the auditory nerve induces reactive gliosis not only in the auditory nerve but also in the cochlear nucleus. Various aspects of hearing loss that occur after surgical treatment for VS can best be explained in terms of reactive gliosis combined with additional pathophysiological mechanisms described previously. We emphasize the need to investigate pathological changes not only in the axons but also in the astrocytes to thoroughly understand the mechanisms responsible.

Methods

Inducing Auditory Nerve Degeneration by Compression

Animal experiments were conducted in accordance with the Guidelines for Animal Experiments at Kyoto University. In our experimental model, the axons of the auditory nerve were quantitatively compressed in the CPA without permanent compromise of the blood supply to the cochlea. This was achieved by intraoperative monitoring of CAPs from the auditory nerve as reported elsewhere.[30,43] Briefly, male Sprague-Dawley rats weighing 400–450 grams each were anesthetized by an intraperitoneal injection of ketamine (100 mg/ml; Sankyo Co.) and xylazine (9 mg/ml; Bayer). After exposing the trunks of the seventh and eighth cranial nerves through right retromastoid craniectomy, simulating the same procedure in humans, an L-shaped stainless-steel wire was placed on the auditory nerve as the CR electrode to compress the auditory nerve and simultaneously record the CAPs (Fig. 1). The only device that directly touched the auditory nerve throughout the experiment was this CR electrode. In several rats, the auditory nerve was identified in the CPA and the wound was closed without compressing the nerve. In these rats, the ABRs were completely preserved, and the histological analyses revealed normal cochleae, auditory nerves, and brainstems (data not shown).

In the experimental animals, as the CR electrode was advanced, the auditory nerve was gradually compressed between the tip of the electrode and the rostroventral edge of the IAM (Fig. 1). The cochlear portion of the eighth cranial nerve is located posterodorsally at the IAM level, so the cochlear nerve was directly and highly selectively injured by the CR electrode with the vestibular and facial nerves preserved anatomically.[43] First, the CR electrode was advanced at the speed of 1 μm/second (Positions 1, 2, and 3) until the CAP flattened (Position 4), termed the "flat point," and was maintained at the flat point for 1 minute before the electrode was finally advanced to compress the auditory nerve. Rats in which the CAP recovered within 60 seconds after the flat point was reached, while the CR electrode was maintained at the flat point, were included in this study to ensure that the IAA was still functionally intact after the flat point had been reached. The flattening of the CAP was caused by impairment of the blood supply to the cochlea through the IAA. Recovery of the IAA caused the CAP to reappear spontaneously, while the CR electrode was maintained at the flat point. The critical time of cochlear ischemia that allows for complete recovery of the CAP has been reported to be 5 minutes or more.[2,40] In this experimental model, the cessation of blood supply to the cochlea never exceeded 1 minute in either of the advancements of the CR electrode.

In Group A, the CR electrode was advanced 200 μm from the flat point to compress the auditory nerve. Six rats in this group were studied 1 week after compression and another 6 rats were studied 8 weeks after compression.

In Group B, the electrode was advanced 400 μm, thus increasing the compression damage to the nerve. The same numbers of animals were studied at the same time intervals.

In both groups, the speed of CR electrode advancement was 10 μm/second during the second advancement (the compression procedure); 60 seconds after the start of the second advancement, the electrode was withdrawn at 110 μm/second. The temporal bone on the right side was treated and the left side was used as a control.

Recordings of ABRs and CAPs of Auditory Nerve

Auditory brainstem responses were recorded between the base of the earlobe of the operative side (right) and the vertex, with the ground electrode at the base of the forelimb. Click stimuli (100 dB sound pressure level) were presented to the right ear at a rate of 9.5 pulses/second through a tube earphone or a hollow ear bar driven by a 100-μsec rectangular pulse wave fed by a stimulator. Evoked potentials were amplified with a bandpass of 50 Hz to 3 kHz and averaged using a processor (Synax 1100, NEC Medical Systems) with a sampling interval of 20 μsec and 500 data points in each recording. The responses to 100 successive clicks were averaged for ABR recordings and stored in a computer. Alternating clicks were used to stimulate the ABR. During the first and second compression procedures, the CAPs were recorded between the tip of the CR electrode and the vertex, with the ground electrode placed at the base of the forelimb. For CAP recordings, the acoustic nerve potentials evoked by 5 successive clicks were averaged and stored in a computer. This rate led to a continuous CAP recording rate

of 1 potential every 2.4 seconds before the flat point. The click was picked up at the exit from the earphone with a microphone (ACO 4016, ACO Pacific) connected to the earphone and amplified with a microphone amplifier (MA3, Tucker-Davis Technologies). It was subsequently transferred to an oscilloscope (Iwatsu DS-8812, Iwatsu Electric) for fast Fourier transform analysis, revealing that the frequency of the tones included in the click ranged up to approximately 5 kHz. In contrast to absolute values of amplitudes of ABR, IPLs are relatively independent of the intensity of the stimulus.[11] We measured IPL between Waves I and II (I–II IPL) and IPL between Waves II and IV (II–IV IPL) to investigate the state of nerve impulse conduction from the cochlea to the brainstem. For statistical analyses, unpaired t-tests were performed using Microsoft Office Excel 2007.

Immunohistochemical Analysis

To prepare the temporal bones, each rat was placed in a state of deep anesthesia and was perfused transaortically with 4% paraformaldehyde in 0.01 M PBS at pH 7.4. The temporal bones were decalcified with 10% EDTA and HCl solution (pH 7.4) for 2–3 weeks.

After decalcification, the temporal bones were embedded in OCT compound (Sakura Finetechnical) and frozen. Serial 8-μm sections were then cut for immunohistochemical analysis. Midmodiolar sections included 4 good cross-sections of the Rosenthal canal (basal, lower middle, upper middle, and apical) and the widest part of the auditory nerve. These sections were mounted on glass slides, washed in PBS, and dried at room temperature for 30 minutes. They were permeabilized and then blocked with 10% goat serum in PBS-T (PBS containing 0.2% Triton X-100) at room temperature for 30 minutes.

To visualize astrocytes in the auditory nerve and cochlear nucleus, anti-GFAP rabbit polyclonal antibody (× 500; DAKO) was applied to the sections and incubated at 4°C for 12 hours followed by washing in PBS-T 3 times for 5 minutes each. A secondary antibody (Alexa Fluor 488 goat anti–rabbit IgG antibody × 500, Molecular Probes, diluted with 10% goat serum in PBS-T) was applied to the sections at room temperature for 1 hour followed by washing in PBS-T twice for 5 minutes each time.

To visualize neurons, anti–beta III-tubulin mouse monoclonal antibody (× 500; Covance Research Products, Berkeley) was used as the primary antibody and Alexa Fluor 594 goat anti–mouse IgG antibody (× 500, Molecular Probes) as the secondary antibody.

For nuclear staining, the sections were incubated in 4′,6-diamidino-2-phenylindole (DAPI, 2 μg/ml, Molecular Probes) solution at room temperature for 15 minutes. After being rinsed in PBS, the samples were mounted onto glass slides and coverslipped with VECTASHIELD mounting medium (Vector Laboratories). A fluorescence microscope system equipped with appropriate filters (Olympus BX50 and BX-FLA) was used for observation, and samples were photographed with a digital camera (Olympus DP10). Confocal images were obtained with a confocal laser-scanning microscope (TCS-SP2 Leica Microsystems). Images used for the figures were processed with Photoshop (version 6.0, Adobe Systems).

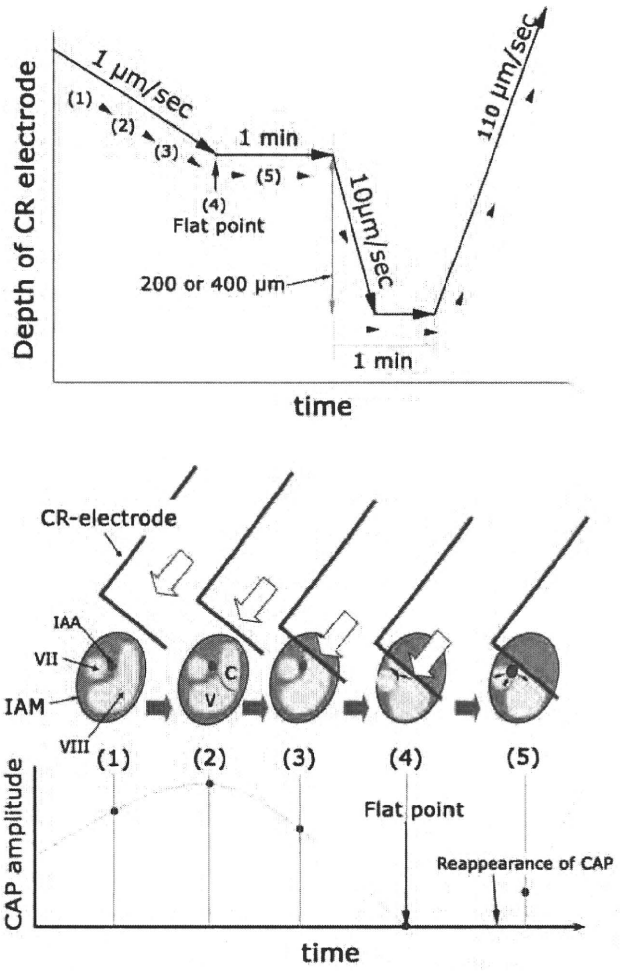

Fig. 1. Mode of advancement of the CR electrode **(upper)** and relationship between electrode depth and amplitude of the auditory nerve CAP during the first advancement of the electrode **(lower)**. **Upper:** First, the CR electrode was advanced at 1 μm/second (CR electrode Positions 1, 2, and 3) until the CAP flattened (Position 4). The CR electrode was maintained at the flat point for 1 minute and then was advanced 200 μm (in Group 1 rats) or 400 μm (in Group 2 rats) at 10 μm/second to compress the auditory nerve; 60 seconds after the start of this advancement, the electrode was withdrawn at 110 μm/second. **Lower:** The IAC contents at the IAM level of the right ear, viewed from the brainstem side toward the cochlea. The CAP amplitude increased as the CR electrode came close to the auditory nerve (Positions 1 and 2) and decreased as the CR electrode continued to be advanced and began to directly compress the auditory nerve due to conduction block of nerve impulses (Position 3). The CAP flattening was caused by impairment of the blood supply to the cochlea through the IAA (Position 4, *small black arrow* indicates collapsed IAA). However, pulsation of the IAA would push the surrounding nerve tissue aside *(small black arrows)*, causing the caliber of the IAA to normalize gradually and the CAP to reappear spontaneously, while the CR electrode was maintained at the flat point (Position 5).

Results

Controls

In a previous paper we demonstrated that a TZ, the interface between the PNS and the CNS portions of the auditory nerve, can be observed even in routine H & E

staining.[44] In our present study the TZ was more clearly observed with anti-GFAP immunostaining because astrocytes are found only in the CNS portion of the auditory nerve (Fig. 2).

At the fundus of the IAC, multiple tiny osseous canals, called the TSF, allow the axons to pass from the Rosenthal canal along the auditory nerve (modiolus) toward the CNS (Figs. 2 and 3).[50]

Throughout the control specimens, the length of the astrocytic processes toward the basal cochlear turn tended to be longer than those toward the middle and apical cochlear turns (Fig. 2 right). It was noted, however, that these astrocytic processes never entered into the TSF in any cochlear turn, even in the basal cochlear turn in controls. With the exception of those in the basal turn, the length of the astrocytic processes never exceeded approximately 75 μm.

Electrophysiological and Morphological Changes After Compression

In rats the CNS portion of the auditory nerve is relatively long, and hence, the TZ is situated within the IAC as in humans (Figs. 2 and 3).[15,53] Because of this anatomical relationship, the compression in the CPA cistern always injured the CNS portion where astrocytes are abundant.

Group A. One week after compression, the general shape of the ABR was preserved but the peak amplitudes were attenuated and the latencies of Waves II, III, and IV were prolonged (Fig. 4). The I–II IPL increased from 0.34 ± 0.03 msec before compression to 0.40 ± 0.03 msec (mean ± SD). The II–IV IPL increased from 0.64 ± 0.03 msec to 0.66 ± 0.04 msec (Fig. 5). The I–II IPL was significantly prolonged after compression ($p < 0.05$) but the II–IV IPL was not. After compression, an unlabeled region was observed just beneath the compression site (Fig. 6). Within this region, GFAP immunoreactivity was lost, indicating the mechanical disruption of the astrocytes. The shape of the TZ was essentially unchanged and the astrocytic outgrowth at the TZ was limited. In the cochlear nucleus we did not observe any change in GFAP staining (data not shown).

Eight weeks after compression the general configuration of the ABR was preserved but the peak amplitude was attenuated and the latencies of Waves II, III, and IV were prolonged (Fig. 7). The latency of the I–II IPL increased from 0.34 ± 0.02 msec to 0.41 ± 0.03 msec ($p < 0.05$) and the II–IV IPL decreased from 0.64 ± 0.01 msec to 0.63 ± 0.03 msec (not significant) (Fig. 5). There was no significant difference in the I–II IPLs between 1 week and 8 weeks after compression. Labeling for GFAP showed that the astrocytic processes elongated enormously from the TZ toward the PNS portion of the auditory nerve (Fig. 8A and B). The length of a substantial number of astrocytic processes was more than 200 μm. The elongated processes ran in parallel with the residual auditory neurons. They entered much further into the TSF in the basal portion of the cochlea compared with the middle cochlear turns (Fig. 8B and C). At the compression site, small, unlabeled areas were observed. Confocal images disclosed a dense meshwork of gliotic tissue at and in the vicinity of the lesion epicenter and fragments of neurons were scattered in this gliotic tissue (Fig. 8D). In the cochlear nucleus, hypertrophic astrocytic processes were abundant around the soma of the neurons (Fig. 8E *single asterisks*) in comparison with the control (Fig. 8F), and in a limited area they formed a meshlike structure of gliotic tissue (Fig. 8E *double asterisks*).

Group B. One week after compression, the ABR was hardly discernible (Fig. 9). Immunohistochemically, a large area unlabeled for GFAP was observed at the compression site (Fig. 10), and it was much larger than that observed in Group A (Fig. 6). The IAC was filled with swollen auditory nerve tissue, a finding not observed in any of the rats in Group A at either time point or in the Group B rats 8 weeks after compression (see below). Astrocytic outgrowth from the TZ was, however, limited (Fig. 10 *large arrowheads*) and in the cochlear nucleus there was no obvious change in GFAP staining (data not shown).

Eight weeks after compression, the peaks of the ABR could not be identified (Fig. 11). The growth of astrocytic processes was much more extensive than in Group A at 8 weeks postcompression (Fig. 12). The length of many processes was more than 300 μm. The astrocytic outgrowth was most evident at the basal portion of the cochlear turn, where the processes elongated and occupied all the orifices of the TSF. Confocal images showed that they ran parallel with the residual auditory neurons within the TSF. In the lesion epicenter, dense gliotic tissue surrounded neural tissue fragments. Similar dense gliotic tissue occupied the cochlear nucleus, where the neurons were tightly surrounded by ramified gliotic tissue. This pathology was only rarely observed in the Group A animals (Fig. 8E). The transverse diameter of the auditory nerve at and proximal to the compression site was reduced considerably, and this finding was more pronounced in this subgroup than in the Group A rats killed at 8 weeks (Figs. 12A and 8A, respectively).

Discussion

In this study we demonstrate for the first time that compression of the auditory nerve induces reactive gliosis not only in the auditory nerve but also in the cochlear nucleus. This can occur even with minimal degradation of the ABR. Thus, reactive gliosis should potentially be regarded as a "third causative factor," in addition to neural and vascular factors, for hearing loss following surgical treatment for VS.

Glial Scar Formation and Degree of Injury

Glial scars are formed in the adult CNS following various insults and constitute a physical and molecular barrier unfavorable to axon survival and regeneration.[6,41,49] In our present study, the gliotic tissue was observed at the lesion epicenter and in the vicinity of the compression site 8 weeks postcompression. Normal tissue architecture was lost, and fragments of auditory neurons were surrounded by reactive astrocytes (Figs. 8D and 12D). Reported ultrastructural findings of degenerating and degenerated

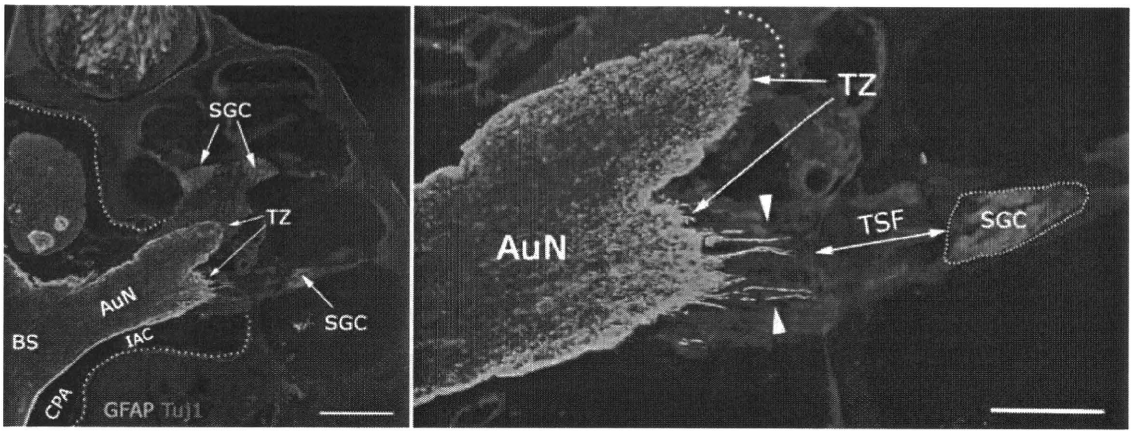

Fig. 2. Photomicrographs showing the TZ of the normal auditory nerve. The interface between the central and peripheral portions of the auditory nerve is clearly observed with anti-GFAP immunostaining *(green)* because of the presence of astrocytes only in the CNS portion of the auditory nerve. Note that the astrocytic processes toward the basal cochlear turn are longer than those toward the other cochlear turns (*arrowheads* in the **right panel**). The astrocytic processes never entered into the TSF in any cochlear turn even in the basal cochlear turn in controls. In this rat, the length of the astrocytic processes from the TZ was less than 75 μm, the longest distance of astrocytic extension in controls in all the cochlear turns except the basal turn (*dotted line* in the **right panel**). The *dotted line* in the **left panel** indicates the border between the intra- and extracranial compartments. Anti-GFAP and anti–beta III-tubulin (clone Tuj1) immunostaining. Bar = 500 μm (left) and 250 μm (right). AuN = auditory nerve; BS = brainstem; SGC = spiral ganglion cell.

axon terminals surrounded and phagocytosed by reactive astrocytes after deafferentation may correspond to our results.[4,10,17,23]

Our results also show that the higher level of compression applied to animals in Group B caused greater degradation of the ABR, increased astrocytic outgrowth from the TZ, higher levels of gliosis in the cochlear nucleus, and larger areas lacking GFAP labeling close to the compression site. In spinal cord injury, the hemorrhagic zone at the lesion epicenter cavitates as a result of necrosis several days after trauma.[22,55] Hemorrhagic foci have been observed previously within the auditory nerve trunk following mechanical trauma.[45] This study shows that they decrease between 1 and 8 weeks after surgery, suggesting invasion by reactive astrocytes. The observed swelling of the auditory nerve within the IAC was much less for low levels of compression and after the longer survival period. Hence, it is likely that swelling occurs only in acute stages of severely compressed auditory nerves, and that it is caused by edema as observed in the optic nerve.[25]

Astrocytic Proliferation and ABR Deterioration

In small experimental animals, Wave I of the ABR is generated from the extracranial (intratemporal bone) portion of the auditory nerve, Wave II reflects synaptic activity in the cochlear nucleus, and the subsequent waves reflect electrical activity in the pons/upper brainstem.[33,46] Because the compression site in our experiments was situated at the IAM, the IPL between Waves I and II was prolonged, but from Wave II through Wave IV the latencies were unaffected.

In our present study, the astrocytic processes elongated conspicuously from the TZ toward the PNS portion of the auditory nerve, ran parallel with the residual auditory neurons, and entered into the TSF, particularly

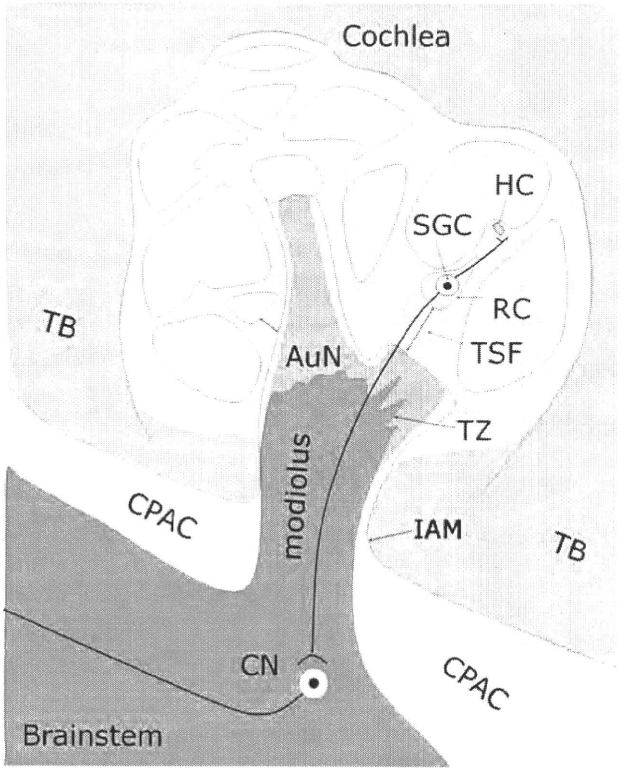

Fig. 3. Schematic illustration showing the anatomical relationships between the auditory nerve and the surrounding structures. The auditory nerve is a bundle of bipolar neurons that form synaptic contacts with the hair cells peripherally and cochlear nucleus cells centrally. The cell bodies of the auditory neurons (spiral ganglion cells) are housed in the Rosenthal canal. The TSF is an osseous canal through which the axons of the auditory nerve pass from the Rosenthal canal to the axis of the auditory nerve (modiolus). CN = cochlear nucleus; CPAC = CPA cistern; HC = hair cell; RC = Rosenthal canal; TB = temporal bone.

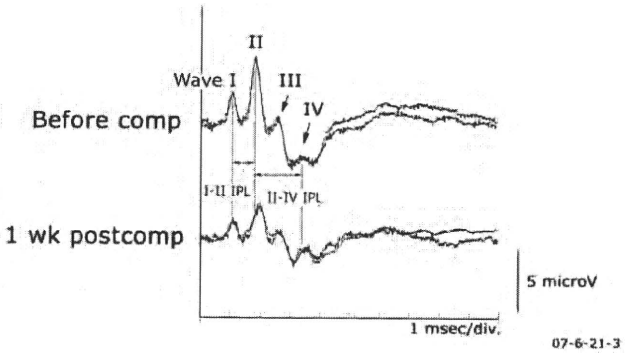

Fig. 4. Auditory brainstem responses in a Group A rat, before and 1 week after compression. The general configuration of the ABR was maintained after compression, but the amplitude of each peak was attenuated and the latencies of Waves II, III, and IV were prolonged. The IPL between Waves I and II (I–II IPL) and that between Waves II and IV (II–IV IPL) before compression are indicated by *doubleheaded horizontal arrows*. Comp = compression.

in the basal region of the cochlea. Massive proliferation of astrocytic processes within the modiolus may physically compress the adjacent nerve fibers, especially within the narrow canals of the TSF. If so, then this could be a cause of hearing loss. Moreover, enhanced glial activity in the region of the cochlear nucleus might have caused both structural and functional changes among synaptic complexes and postsynaptic neurons.[14,16,48] Progressive degeneration of axons has been reported to occur over 8 months and more than 1 year after peripheral insult to the auditory nerve/cochlear nucleus (noise-induced hair cell damage) and spinal cord injury, respectively.[35,57] Thus, the attenuation of Wave II of the ABR may have been caused both by reactive gliosis related to cochlear nucleopathy and by reduction of auditory nerve activity in the cochlear nucleus.

Within Group A, statistically significant differences in the I–II IPLs were not observed between 1 and 8 weeks after compression. However, some auditory nerve degeneration must have developed without being detected in the ABR recordings. Our fast Fourier transform analysis revealed that the click that we used included frequencies up to approximately 5 kHz. The stimulator used was designed for use in humans, and its power spectrum normally stimulates the apical, middle, and upper basal turns of the cochlea; in rats, however, it stimulates only approximately one-quarter of the length of the cochlea.[11,37,60] Thus, the ABRs in our experiments did not cover the potential electrophysiological changes associated with the auditory nerve dysfunction due to the massive outgrowth of astrocytic processes in the lower apical, middle, and basal turns. In one study on rats in which the cochlea was surgically removed, GFAP immunoreactivity increased in the cochlear nuclei 2 days after the surgery, remained intense for 3–8 days, and then declined by Day 21.[12] In another study, the GFAP reaction occurred on Day 1, increased in intensity at Days 4–21, and then remained elevated until Day 45 in the cochlear nucleus (the longest observation time in the study).[8] Our results suggest that

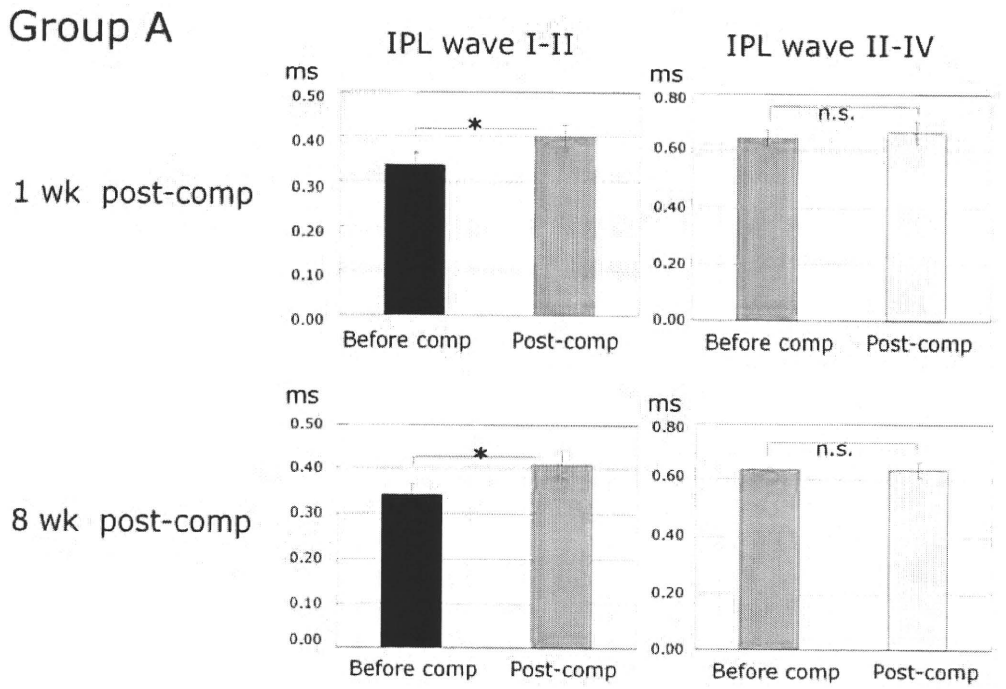

Fig. 5. Bar graphs showing the mean IPLs (± 1 SD) between Waves I and II (I–II IPL) and between Waves II and IV (II–IV IPL), 1 week and 8 weeks after compression in Group A. The I–II IPL was significantly prolonged after compression but the II–IV IPL was not. There was no significant difference between the I–II IPL at 1 week and that at 8 weeks postcompression. ms = msec; n.s. = not significant. * $p < 0.05$.

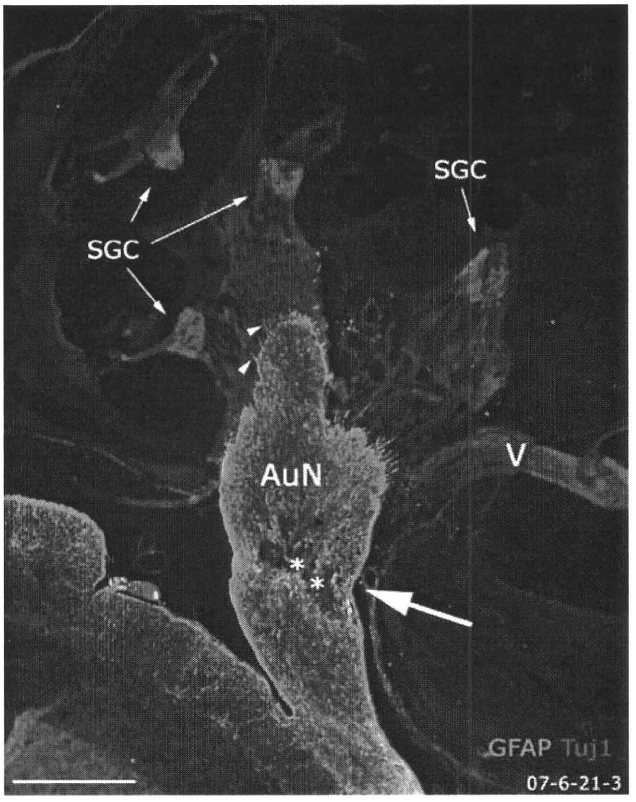

FIG. 6. Photomicrograph showing morphological changes in the auditory nervous system 1 week after compression in Group A (the same rat as in Fig. 4). A GFAP-negative region *(asterisks)* was observed at the compression site *(arrow)*. The shape of the TZ was essentially unchanged *(arrowheads)*. Anti-GFAP and anti–beta III-tubulin (clone Tuj1) immunostaining. Bar = 500 μm. V = vestibular nerve.

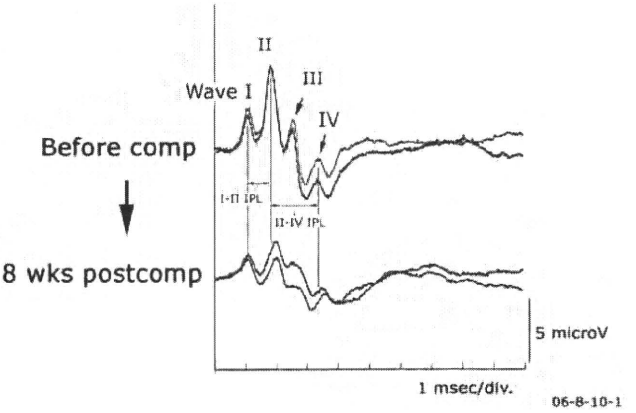

FIG. 7. Auditory brainstem response in a Group A rat, before and 8 weeks after compression. The amplitude was attenuated, but each peak of the ABR was preserved while the latencies of Waves II, III, and IV were prolonged. The I–II IPL and II–IV IPL before compression are indicated by *doubleheaded arrows*.

reactive gliosis continues at least to the 8th week post-compression, and longer-term studies are needed to describe the full consequences of the response.

Clinical Extrapolations

Various clinical observations can be explained by reactive gliosis combined with the previously reported pathophysiological mechanisms. Several reports have demonstrated that the presence of adhesion in the interface between the auditory nerve and the tumor is the most significant negative prognostic factor in hearing preservation surgery, regardless of tumor size.[24,36,51,61] The less adhesion, the less mechanical force needed to separate the auditory nerve from the tumor surface, leading not only to less trauma-induced auditory nerve degeneration but also to less reactive gliosis.

"Cochlear nucleopathy" may "naturally" occur as a VS increases in volume. As the cochlear nuclei are located at the entrance of the fourth ventricle[1] and the shape of the fourth ventricle is inevitably distorted in accordance with tumor growth, the cochlear nuclei cannot escape from the effects of mechanical stress and reactive gliosis. In patients with neurofibromatosis Type 2, the outcome of auditory brainstem implant placement was less favorable in those cases in which the VS compressed and distorted the brainstem than in those in which it did not.[31] In the former, reactive astrocytic proliferation in the cochlear nuclei may have modified synaptic organization leading to less effectiveness of the implant, although larger tumors can be expected to cause more advanced degeneration than smaller ones.

There are some caveats with respect to extrapolation from our results to the situation in human patients. First, the length of the auditory nerve differs markedly between rats and humans. In rats the cisternal portion is approximately 0.5 mm at most (Fig. 2), whereas in humans it is approximately 10–15 mm.[26,34,54] Reactive gliosis may be more severe where the compression site is so much closer to the brainstem.[29,42] Second, in our study the changes to the ABR were created on purpose by traumatizing the "normal" auditory nerve. Under clinical conditions, trauma to the normal auditory nerve may be very rare. In the clinical setting, the ABR configuration in patients with VS is often already distorted before surgical intervention, with the tumor mass causing auditory nerve dysfunction through mechanical compression. This is especially the case with respect to the intracanalicular portion of the auditory nerve. In a study in which the intracanalicular pressure was directly measured in the patients with VS, the pressure within the IAC was significantly elevated, and the authors concluded that pressure from tumor growth in the IAC might be responsible for hearing loss.[3] The morbid auditory nerve in the patients with VS could be significantly more sensitive to the same insult than the normal auditory nerve.[27] Third, we observed ABR decline and remarkable astrocytic proliferation 8 weeks after compression. In contrast, delayed hearing loss has been reported years after surgery in patients who have undergone VS surgery with preserved hearing.[5,9,18,32,58,59] Therefore, our results may be better applied to "subacute" hearing loss in VS surgery. Typically, these patients wake up with hearing after surgery but suffer hearing loss 1–2 months later. However, the time course in gliosis may be different in humans and rats, and it is important to carry

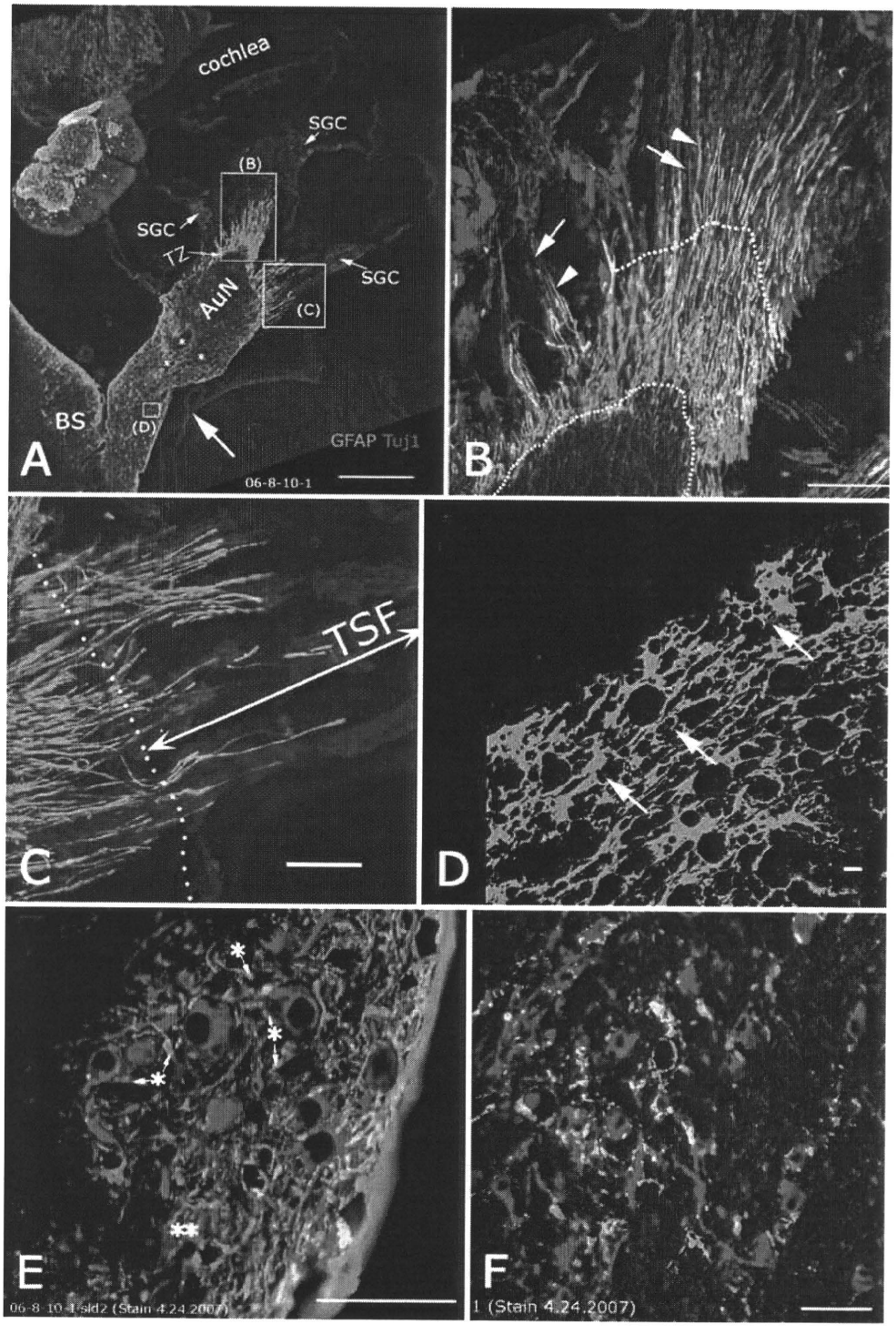

Fig. 8. Morphological changes in the auditory nervous system 8 weeks after compression in Group A (the same rat as in Fig. 7). The astrocytic processes elongated enormously from the TZ toward the periphery (**A and B**). The length of many astrocytic processes was more than 200 μm from the TZ (*dotted lines* in **B**) and they ran parallel with the residual auditory neurons (the *arrowhead* in **B** indicates an astrocytic process and the *arrows*, auditory neurons). The astrocytic processes penetrated the TSF more deeply in the basal portion of the cochlea **(C)** than in the middle portion **(B)**. (Panels **B and C** are enlargements of areas indicated by "(B)" and "(C)" in **panel A**.) At the compression site (*large arrow* in **A**), small, unlabeled areas were observed (*asterisks* in **A**). At and in the vicinity of the lesion epicenter, a dense meshwork of gliotic tissue containing the fragments of neurons (*arrows* in **D**) was observed (the area indicated by "(D)" in **panel A** is enlarged in **panel D**). Hypertrophic astrocytic processes were observed in the cochlear nucleus (*single asterisks* in **E**). Meshlike structure of gliotic tissue was occasionally seen (*double asterisks* in **E**). **F:** Cochlear nucleus region in control. Anti-GFAP and anti–beta III-tubulin (clone Tuj1) immunostaining. Bar = 500 μm (A), 100 μm (B), 100 μm (C), 10 μm (D), 50 μm (E), and 50 μm (F).

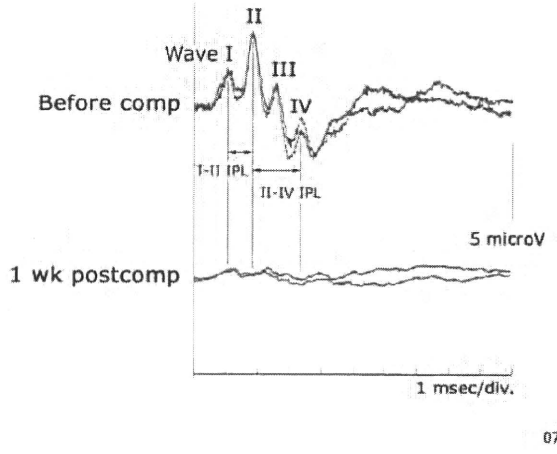

FIG. 9. Auditory brainstem responses in a Group B rat before and 1 week after compression. All the components of ABR were hardly discernible after compression. The I–II IPL and II–IV IPL before compression are indicated by *doubleheaded arrows.*

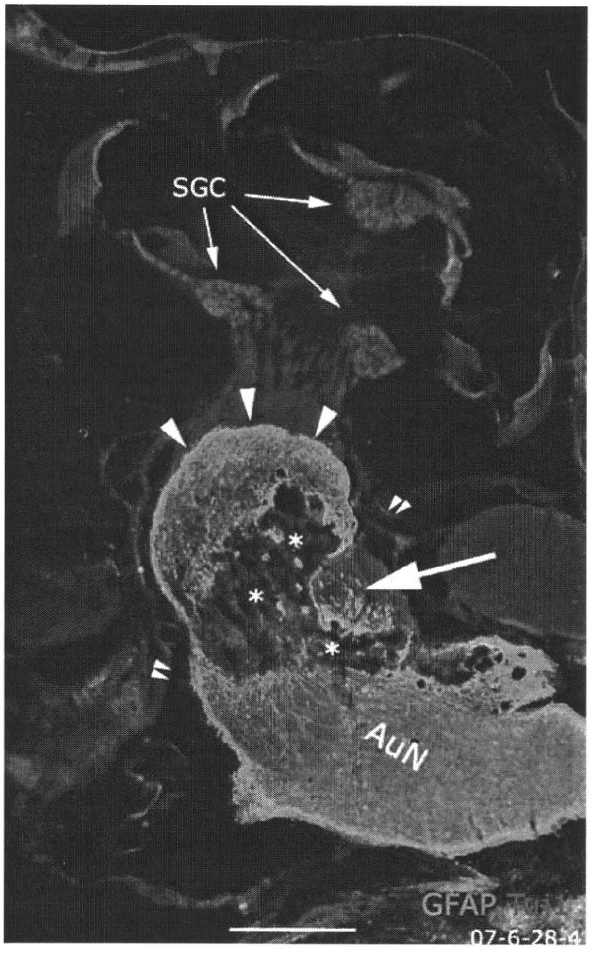

FIG. 10. Morphological changes in the auditory nerve 1 week after compression in a Group B rat (the same animal as in Fig. 9). A large area unlabeled for GFAP *(asterisks)* was observed at the compression site *(arrow)* (compare with Fig. 6). The IAC was filled with swollen auditory nerve tissue. Astrocytic outgrowth from the TZ was limited *(large arrowheads). Small double arrowheads* indicate the IAM. Anti-GFAP and anti–beta III-tubulin (clone Tuj1) immunostaining. Bar = 500 μm. Original magnification × 2.

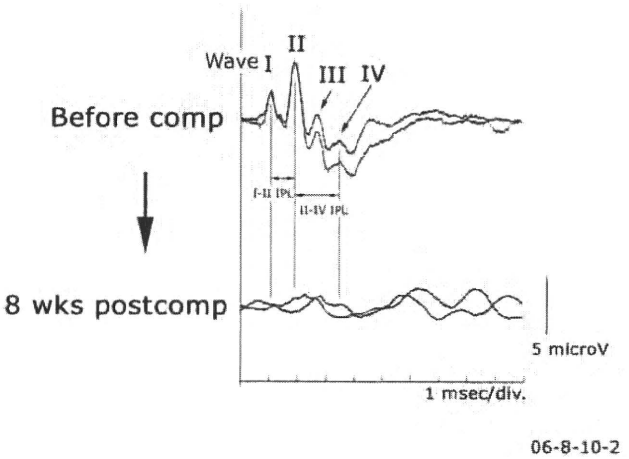

FIG. 11. Auditory brainstem responses in a Group B rat before and 8 weeks after compression. The waveform was not visible after compression. The I–II IPL and II–IV IPL before compression are indicated by *doubleheaded arrows.*

out short- and long-term studies of sequential ABR tracings following surgery in human patients.

Conclusions

We applied compression, a constituent mechanical factor in complex operative procedures, to the auditory nerve of rats while recording ABRs to measure the related hearing loss quantitatively. We found for the first time that a substantial reactive gliosis occurs in both the peripheral and central auditory pathways within 1–8 weeks and is associated with significant degradation of the ABR. This finding warrants further research to test the possibility that in the longer term the gliosis may correlate with and may even cause continued hearing loss. Reactive gliosis may be a primary cause of progressive hearing loss following microsurgical treatment for VS.

Disclosure

The authors report no conflict of interest concerning the materials or methods used in this study or the findings specified in this paper. This study was supported by the Ministry of Education, Culture, Sports, Science and Technology (Japan), the General Insurance Association of Japan, and the Univers Foundation (Japan).

Author contributions to the study and manuscript preparation include the following. Conception and design: T Sekiya. Acquisition of data: T Sekiya, M Matsumoto, K Ono, S Kada, H Ogita, RT Horie, A Viola. Analysis and interpretation of data: T Sekiya, K Ono, MC Holley. Drafting the article: T Sekiya. Critically revising the article: T Sekiya, MC Holley. Reviewed final version of the manuscript and approved it for submission: T Sekiya, M Matsumoto, K Kojima, K Ono, YS Kikkawa, S Kada, H Ogita, RT Horie, A Viola, MC Holley, J Ito. Statistical analysis: T Sekiya. Study supervision: J Ito.

Acknowledgments

The authors appreciate Dr. Agneta Viberg for her useful discussion, and Keiko Nishio, Koichiro Shimomura, Kazumi Sugimoto, and Masashi Higashino for their technical assistance and animal care.

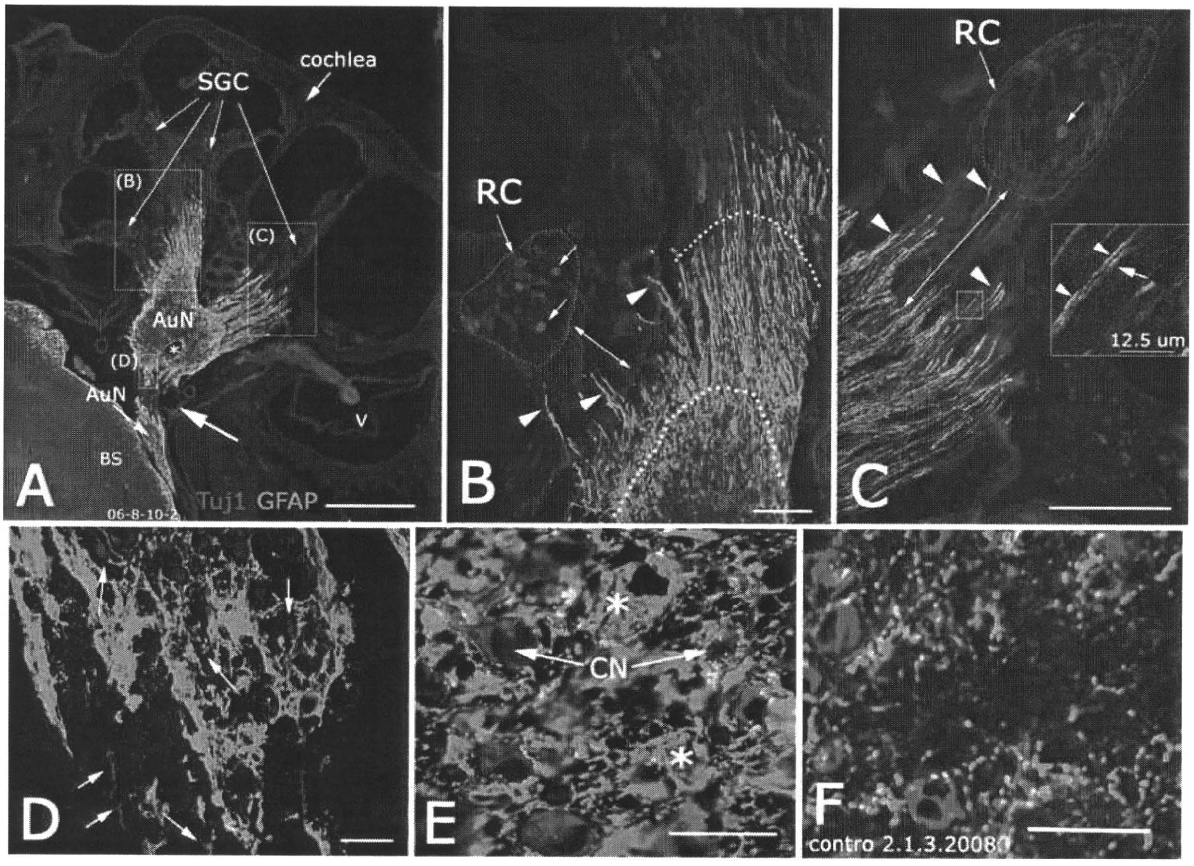

Fig. 12. Morphological changes in the auditory nervous system 8 weeks after compression in a Group B rat (the same animal as in Fig. 11). Extensive astrocytic outgrowth from the TZ was evident (**A–C**). The length of many astrocytic processes was more than 300 μm from the TZ (*dotted lines* in **B**). In the basal turn of the cochlea where the astrocytic outgrowth was greatest, the elongated processes occupied all the orifices of the TSF (*arrowheads* in **C**). The rectangle in C is enlarged in the **inset**; the astrocytic processes (indicated by *arrowheads*) ran parallel with the residual auditory neurons (indicated by *arrow*). In the lesion epicenter, dense plexiform gliotic tissue surrounded neural tissue fragments (*arrows* in **D**). Multiple, small areas unlabeled for GFAP were observed at the compressed site (*asterisk* in A). In the cochlear nucleus, neurons were surrounded by dense gliotic tissue (*asterisks* in **E**; cochlear nucleus region in control, **F**). The transverse diameter of the auditory nerve at and proximal to the compression site was reduced in comparison with that in the Group A rats at 8 weeks postcompression (Fig. 8). The *small arrows* in the Rosenthal canals in **B and C** indicate the residual spiral ganglion cells after compression. Anti-GFAP and anti–beta III-tubulin (clone Tuj1) immunostaining. Bar = 500 μm (A), 100 μm (B), 200 μm (C), 25 μm (D), 25 μm (E), and 25 μm (F).

References

1. Abe H, Rhoton AL Jr: Microsurgical anatomy of the cochlear nuclei. **Neurosurgery 58:**728–739, 2006
2. Asai Y, Umemura K, Nakashima M: Reversibility of compound action potential during the acute phase after transitory local ischemia. **Ann Otol Rhinol Laryngol 105:**472–475, 1996
3. Badie B, Pyle GM, Nguyen PH, Hadar EJ: Elevation of internal auditory canal pressure by vestibular schwannomas. **Otol Neurotol 22:**696–700, 2001
4. Bechmann I, Nitsch R: Astrocytes and microglial cells incorporate degenerating fibers following entorhinal lesion: a light, confocal, and electron microscopical study using a phagocytosis-dependent labeling technique. **Glia 20:**145–154, 1997
5. Betchen SA, Walsh J, Post KD: Long-term hearing preservation after surgery for vestibular schwannoma. **J Neurosurg 102:**6–9, 2005
6. Buffo A, Rite I, Tripathi P, Lepier A, Colak D, Horn AP, et al: Origin and progeny of reactive gliosis: A source of multipotent cells in the injured brain. **Proc Natl Acad Sci U S A 105:**3581–3586, 2008
7. Burnett MG, Zager EL: Pathophysiology of peripheral nerve injury: a brief review. **Neurosurg Focus 16(5):**E1, 2004
8. Campos-Torres A, Touret M, Vidal PP, Barnum S, de Waele C: The differential response of astrocytes within the vestibular and cochlear nuclei following unilateral labyrinthectomy or vestibular afferent activity blockade by transtympanic tetrodotoxin injection in the rat. **Neuroscience 130:**853–865, 2005
9. Chee GH, Nedzelski JM, Rowed D: Acoustic neuroma surgery: the results of long-term hearing preservation. **Otol Neurotol 24:**672–676, 2003
10. Cheng HW, Jiang T, Brown SA, Pasinetti GM, Finch CE, McNeill TH: Response of striatal astrocytes to neuronal deafferentation: an immunocytochemical and ultrastructural study. **Neuroscience 62:**425–439, 1994
11. Chiappa KH: Brain stem auditory evoked potentials: methodology, in Chiappa KH (ed): **Evoked Potentials in Clinical Medicine, ed 2.** New York: Raven Press, 1990, pp 173–221

12. de Waele C, Campos Torres A, Josset P, Vidal PP: Evidence for reactive astrocytes in rat vestibular and cochlear nuclei following unilateral inner ear lesion. **Eur J Neurosci 8:**2006–2018, 1996
13. Eng LF, Ghirnikar RS, Lee YL: Glial fibrillary acidic protein: GFAP-thirty-one years (1969–2000). **Neurochem Res 25:**1439–1451, 2000
14. Eriksson NP, Persson JK, Svensson M, Arvidsson J, Molander C, Aldskogius H: A quantitative analysis of the microglial cell reaction in central primary sensory projection territories following peripheral nerve injury in the adult rat. **Exp Brain Res 96:**19–27, 1993
15. Fraher JP, Delanty FJ: The development of the central-peripheral transitional zone of the rat cochlear nerve. A light microscopic study. **J Anat 155:**109–118, 1987
16. Garrison CJ, Dougherty PM, Kajander KC, Carlton SM: Staining of glial fibrillary acidic protein (GFAP) in lumbar spinal cord increases following a sciatic nerve constriction injury. **Brain Res 565:**1–7, 1991
17. Gentschev T, Sotelo C: Degenerative patterns in the ventral cochlear nucleus of the rat after primary deafferentation. An ultra-structural study. **Brain Res 62:**37–60, 1973
18. Goel A, Sekhar LN, Langheinrich W, Kamerer D, Hirsch B: Late course of preserved hearing and tinnitus after acoustic neurilemoma surgery. **J Neurosurg 77:**685–689, 1992
19. Graeber MB, Kreutzberg GW: Astrocytes increase in glial fibrillary acidic protein during retrograde changes of facial motor neurons. **J Neurocytol 15:**363–373, 1986
20. Johnsson LG, Hawkins JE Jr, Rouse RC: Sensorineural and vascular changes in an ear with acoustic neurinoma. **Am J Otolaryngol 5:**49–59, 1984
21. Julow J, Szeifert GT, Bálint K, Nyáry I, Nemes Z: The role of microglia/macrophage system in the tissue response to I-125 interstitial brachytherapy of cerebral gliomas. **Neurol Res 29:**233–238, 2007
22. Kakulas BA: The applied neuropathology of human spinal cord injury. **Spinal Cord 37:**79–88, 1999
23. Kapadia SE, LaMotte CC: Deafferentation-induced alterations in the rat dorsal horn: I. Comparison of peripheral nerve injury vs. rhizotomy effects on presynaptic, postsynaptic, and glial processes. **J Comp Neurol 266:**183–197, 1987
24. Koos W, Perneczky A: Suboccipital approach to acoustic neurinomas with emphasis on preservation of facial nerve and cochlear nerve function, in Rand RW (ed): **Microneurosurgery, ed 3.** St. Louis: CV Mosby, 1985, pp 335–365
25. Kountakis SE, Maillard AA, Urso R, Stiernberg CM: Endoscopic approach to traumatic visual loss. **Otolaryngol Head Neck Surg 116:**652–655, 1997
26. Lang J Jr, Ohmachi N, Lang J Sr: Anatomical landmarks of the Rhomboid fossa (floor of the 4th ventricle), its length and its width. **Acta Neurochir (Wien) 113:**84–90, 1991
27. Lapsiwala SB, Pyle GM, Kaemmerle AW, Sasse FJ, Badie B: Correlation between auditory function and internal auditory canal pressure in patients with vestibular schwannomas. **J Neurosurg 96:**872–876, 2002
28. Liu L, Rudin M, Kozlova EN: Glial cell proliferation in the spinal cord after dorsal rhizotomy or sciatic nerve transection in the adult rat. **Exp Brain Res 131:**64–73, 2000
29. Liu PH, Yang LH, Wang TY, Wang YJ, Tseng GF: Proximity of lesioning determines response of facial motoneurons to peripheral axotomy. **J Neurotrauma 23:**1857–1873, 2006
30. Matsumoto M, Sekiya T, Kojima K, Ito J: An animal experimental model of auditory neuropathy induced in rats by auditory nerve compression. **Exp Neurol 210:**248–256, 2008
31. Matthies C, Thomas S, Moshrefi M, Lesinski-Schiedat A, Frohne C, Battmer RD, et al: Auditory brainstem implants: current neurosurgical experiences and perspective. **J Laryngol Otol Suppl 27:**32–36, 2000
32. McKenna MJ, Halpin C, Ojemann RG, Nadol JB Jr, Montgomery WW, Levine RA, et al: Long-term hearing results in patients after surgical removal of acoustic tumors with hearing preservation. **Am J Otol 13:**134–136, 1992
33. Møller AR, Burgess J: Neural generators of the brain-stem auditory evoked potentials (BAEPs) in the rhesus monkey. **Electroencephalogr Clin Neurophysiol 65:**361–372, 1986
34. Møller AR, Jannetta P, Bennett M, Møller MB: Intracranially recorded responses from the human auditory nerve: new insights into the origin of brain stem evoked potentials (BSEPs). **Electroencephalogr Clin Neurophysiol 52:**18–27, 1981
35. Morest DK, Kim J, Potashner SJ, Bohne BA: Long-term degeneration in the cochlear nerve and cochlear nucleus of the adult chinchilla following acoustic overstimulation. **Microsc Res Tech 41:**205–216, 1998
36. Moriyama T, Fukushima T, Asaoka K, Roche PH, Barrs DM, McElveen JT Jr: Hearing preservation in acoustic neuroma surgery: importance of adhesion between the cochlear nerve and the tumor. **J Neurosurg 97:**337–340, 2002
37. Müller M: Frequency representation in the rat cochlea. **Hear Res 51:**247–254, 1991
38. Pekny M: Astrocytic intermediate filaments: lessons from GFAP and vimentin knock-out mice. **Prog Brain Res 132:** 23–30, 2001
39. Pekny M, Wilhelmsson U, Bogestål YR, Pekna M: The role of astrocytes and complement system in neural plasticity. **Int Rev Neurobiol 82:**95–111, 2007
40. Perlman HB, Kimura R, Fernandez C: Experiments on temporary obstruction of the internal auditory artery. **Laryngoscope 69:**591–613, 1959
41. Ridet JL, Malhotra SK, Privat A, Gage FH: Reactive astrocytes: cellular and molecular cues to biological function. **Trends Neurosci 20:**570–577, 1997
42. Salvador-Silva M, Vidal-Sanz M, Villegas-Pérez MP: Microglial cells in the retina of Carassius auratus: effects of optic nerve crush. **J Comp Neurol 417:**431–447, 2000
43. Sekiya T, Hatayama T, Shimamura N, Suzuki S: An in vivo quantifiable model of cochlear neuronal degeneration induced by central process injury. **Exp Neurol 161:**490–502, 2000
44. Sekiya T, Kojima K, Matsumoto M, Holley MC, Ito J: Rebuilding lost hearing using cell transplantation. **Neurosurgery 60:**417–433, 2007
45. Sekiya T, Møller AR: Cochlear nerve injuries caused by cerebellopontine angle manipulations. An electrophysiological and morphological study in dogs. **J Neurosurg 67:**244–249, 1987
46. Shaw NA: The auditory evoked potential in the rat—a review. **Prog Neurobiol 31:**19–45, 1988
47. Shelton C, Hitselberger WE, House WF, Brackmann DE: Hearing preservation after acoustic tumor removal: long-term results. **Laryngoscope 100:**115–119, 1990
48. Shortland P, Woolf CJ: Chronic peripheral nerve section results in a rearrangement of the central axonal arborizations of axotomized A beta primary afferent neurons in the rat spinal cord. **J Comp Neurol 330:**65–82, 1993
49. Stensaas LJ, Partlow LM, Burgess PR, Horch KW: Inhibition of regeneration: the ultrastructure of reactive astrocytes and abortive axon terminals in the transition zone of the dorsal root. **Prog Brain Res 71:**457–468, 1987
50. Stjernholm C, Muren C: Dimensions of the cochlear nerve canal: a radioanatomic investigation. **Acta Otolaryngol 122:** 43–48, 2002
51. Strauss C, Bischoff B, Romstöck J, Rachinger J, Rampp S, Prell J: Hearing preservation in medial vestibular schwannomas. **J Neurosurg 109:**70–76, 2008
52. Sumner BE, Sutherland FI: Quantitative electron microscopy on the injured hypoglossal nucleus in the rat. **J Neurocytol 2:**315–328, 1973
53. Tarlov IM: Structure of the nerve root. II. Differentiation of sensory from motor roots: observations on identification of

function in roots of mixed cranial nerves. **Arch Neurol Psychiatry 37:**1338–1355, 1937
54. Tatagiba M, Matthies C, Samii M: Microendoscopy of the internal auditory canal in vestibular schwannoma surgery. **Neurosurgery 38:**737–740, 1996
55. Tator CH: Review of treatment trials in human spinal cord injury: issues, difficulties, and recommendations. **Neurosurgery 59:**957–987, 2006
56. Tetzlaff W, Graeber MB, Bisby MA, Kreutzberg GW: Increased glial fibrillary acidic protein synthesis in astrocytes during retrograde reaction of the rat facial nucleus. **Glia 1:**90–95, 1988
57. Totoiu MO, Keirstead HS: Spinal cord injury is accompanied by chronic progressive demyelination. **J Comp Neurol 486:**373–383, 2005
58. Tucci DL, Telian SA, Kileny PR, Hoff JT, Kemink JL: Stability of hearing preservation following acoustic neuroma surgery. **Am J Otol 15:**183–188, 1994
59. Umezu H, Aiba T, Tsuchida S, Seki Y: Early and late postoperative hearing preservation in patients with acoustic neuromas. **Neurosurgery 39:**267–272, 1996
60. Viberg A, Canlon B: The guide to plotting a cochleogram. **Hear Res 197:**1–10, 2004
61. Yong RL, Westerberg BD, Dong C, Akagami R: Length of tumor-cochlear nerve contact and hearing outcome after surgery for vestibular schwannoma. **J Neurosurg 108:**105–110, 2008

Manuscript submitted December 6, 2009.
Accepted February 16, 2010.
Please include this information when citing this paper: published online April 2, 2010; DOI: 10.3171/2010.2.JNS091817.

Address correspondence to: Tetsuji Sekiya, M.D., Department of Otolaryngology, Head and Neck Surgery, Kyoto University Graduate School of Medicine, Sakyou-ku, Kyoto, 606-8507 Japan. email: tsekiya@ent.kuhp.kyoto-u.ac.jp.

Hearing Research 270 (2010) 110–118

Contents lists available at ScienceDirect

Hearing Research

journal homepage: www.elsevier.com/locate/heares

Research paper

Salicylate restores transport function and anion exchanger activity of missense pendrin mutations

Kenji Ishihara [a,b], Shuhei Okuyama [a], Shun Kumano [a], Koji Iida [a], Hiroshi Hamana [a], Michio Murakoshi [a], Toshimitsu Kobayashi [c], Shinichi Usami [d], Katsuhisa Ikeda [e], Yoichi Haga [f], Kohei Tsumoto [g], Hiroyuki Nakamura [h], Noriyasu Hirasawa [i], Hiroshi Wada [a,*]

[a] Department of Bioengineering and Robotics, Graduate School of Engineering, Tohoku University, 6-6-01, Aoba, Aramaki, Aoba-ku, Sendai, Miyagi 980-8579, Japan
[b] Laboratory of Medical Science, Course for School Nurse Teacher, Faculty of Education, Ibaraki University, 310-8512, Japan
[c] Department of Otolaryngology Head and Neck Surgery, Graduate School of Medicine, Tohoku University, 980-8575, Japan
[d] Department of Otorhinolaryngology, Shinshu University School of Medicine, 390-8621, Japan
[e] Department of Otorhinolaryngology, Juntendo University School of Medicine, 113-8421, Japan
[f] Department of Biomedical Engineering, Graduate School of Biomedical Engineering, Tohoku University, 980-8579, Japan
[g] Department of Medical Genome Sciences, Graduate School of Frontier Sciences, The University of Tokyo, 277-8562, Japan
[h] Department of Chemistry, Faculty of Science, Gakusyuin University, 171-8588, Japan
[i] Laboratory of Pharmacotherapy of Life-Style Related Diseases, Graduate School of Pharmaceutical Sciences, Tohoku University, 980-8578, Japan

ARTICLE INFO

Article history:
Received 15 April 2010
Received in revised form
26 August 2010
Accepted 30 August 2010
Available online 6 September 2010

ABSTRACT

The *SLC26A4* gene encodes the transmembrane protein pendrin, which is involved in the homeostasis of the ion concentration of the endolymph of the inner ear, most likely by acting as a chloride/bicarbonate transporter. Mutations in the *SLC26A4* gene cause sensorineuronal hearing loss. However, the mechanisms responsible for such loss have remained unknown. Therefore, in this study, we focused on the function of ten missense pendrin mutations (p.P123S (Pendred syndrome), p.M147V (NSEVA), p.K369E (NSEVA), p.A372V (Pendred syndrome/NSEVA), p.N392Y (Pendred syndrome), p.C565Y (NSEVA), p.S657N (NSEVA), p.S666F (NSEVA), p.T721M (NSEVA) and p.H723R (Pendred syndrome/NSEVA)) reported in Japanese patients, and analyzed their cellular localization and anion exchanger activity using HEK293 cells transfected with each mutant gene. Immunofluorescent staining of the cellular localization of the pendrin mutants revealed that p.K369E and p.C565Y, as well as wild-type pendrin, were transported to the plasma membrane, while 8 other mutants were retained in the cytoplasm. Furthermore, we analyzed whether salicylate, as a pharmacological chaperone, restores normal plasma membrane localization of 8 pendrin mutants retained in the cytoplasm to the plasma membrane. Incubation with 10 mM of salicylate of the cells transfected with the mutants induced the transport of 4 pendrin mutants (p.P123S, p.M147V, p.S657Y and p.H723R) from the cytoplasm to the plasma membrane and restored the anion exchanger activity. These findings suggest that salicylate might contribute to development of a new method of medical treatment for sensorineuronal hearing loss caused by the mutation of the deafness-related proteins, including pendrin.

1. Introduction

The auditory system consists of three parts: the outer ear, middle ear and inner ear. Pendrin, which is encoded by the *PDS* (*SLC26A4*) gene, is a 780 amino acid, an 85.7 kDa membrane protein having 12 putative transmembrane domains, and is mainly expressed in the inner ear, thyroid gland and kidney (Everett et al., 1997). In the inner ear, pendrin is detected in the apical membrane of the endolymphatic duct, endolymphatic sac and various cells which compose the cochlea (Yoshino et al., 2004). Pendrin belongs to the *solute carrier 26A* (*SLC26A*) family, which is a group of proteins acting as multifunctional anion exchangers, and transports anions of Cl^-, I^-, $HCO3^-$ and formate (Scott et al., 1999; Mount and Romero, 2004; Wangemann et al., 2007; Kopp et al., 2008). Pendrin is thought to play an important role in the inner ear as a $Cl^-/HCO3^-$

Abbreviations: 7-AAD, 7-amino-actinomycin D; NASEVA, non-syndromic hearing loss with enlarged vestibular aqueduct; SLC26A, solute carrier 26A.

* Corresponding author. Tel.: +81 22 795 6938; fax: +81 22 795 6939.
E-mail address: wada@cc.mech.tohoku.ac.jp (H. Wada).

0378-5955/$ – see front matter © 2010 Elsevier B.V. All rights reserved.
doi:10.1016/j.heares.2010.08.015

transporter involved in the conditioning of ion concentration of the endolymphatic fluid (Mount and Romero, 2004; Wangemann et al., 2007). The loss of pendrin in *Slc26A4*$^{-/-}$ mice, which is a model for Pendred syndrome, results in failure of $HCO3^-$ secretion into endolymph, leading to hearing loss via acidification of endolymph and inhibition of Ca^{2+} reabsorption (Royaux et al., 2001; Wangemann et al., 2007).

More than 150 different mutations of the *PDS* gene have been found in humans so far. These mutations are responsible for Pendred syndrome, which is an autosomal recessive disorder characterized by sensorineuronal hearing loss, goiter and a partial defect in iodide organification, and for non-syndromic hearing loss with an enlarged vestibular aqueduct (NSEVA) (Everett et al., 1997; Kopp, 1999; Dossena et al., 2009). In Japanese, 18 point mutations of the *PDS* gene, i.e., 10 missense mutations, one stop mutation, four frameshift mutations, and three splice site mutations, are reported to lead to these disorders (Tsukamoto et al., 2003). Although Pendred syndrome is thought to account for up to 10% of all cases of syndromic hearing loss, no effective therapy for this syndrome has been established.

Abnormal protein folding or trafficking is associated with various diseases (Thomas et al., 1995; Taubes, 1996; Welch and Brown, 1996). Although, in general, newly synthesized membrane-associated and secreted proteins are translocated to the endoplasmic reticulum, where folding is facilitated by interaction of various endogenous chaperons, abnormal proteins produced by missense mutations are retained in the endoplasmic reticulum by misfolding (Ulloa-Aguirre et al., 2004). It is suggested that such retention and defective plasma membrane targeting of pendrin mutants play a key role in the pathogenesis of Pendred syndrome (Rotman-Pikielny et al., 2002; Dossena et al., 2009). Pharmacological rescue is one method of salvaging these defective proteins by low molecular compounds such as IN3 as chaperones (Conn et al., 2002; Ulloa-Aguirre et al., 2004). Pharmacological chaperones correct errors in folding and restore activity by reestablishing correct protein routing (Ulloa-Aguirre et al., 2004). It has been reported that the misfolded mutants of membrane proteins such as V2 vasopressin receptor, P-glycoprotein and GnRH receptor can be rescued by this method (Loo and Clarke, 1997; Morello et al., 2000; Janovick et al., 2002). Therefore, it is possible that recovery of pendrin mutants by some compounds could improve the condition of Pendred syndrome and NSEVA.

Recently, we have reported that salicylate, which binds to prestin with high affinity (Tunstall et al., 1995; Kakehata and Santos-Sacchi, 1996), induces the translocation of prestin mutants to the plasma membrane from the cytoplasm (Kumano et al., 2010). Prestin is a member of the *SLC26A* gene family including pendrin, and there is approximately a 45% similarity between these proteins in amino acid sequences. Therefore, we hypothesized that pendrin mutants retained in the cytoplasm are induced to translocate to the plasma membrane by salicylate and the function is restored.

In this study, we focused on the 10 missense pendrin mutations (p.P123S (Pendred syndrome), p.M147V (NSEVA), p.K369E (NSEVA), p.A372V (Pendred syndrome/NSEVA), p.N392Y (Pendred syndrome), p.C565Y (NSEVA), p.S657N (NSEVA), p.S666F (NSEVA), p.T721M (NSEVA) and p.H723R (Pendred syndrome/NSEVA)) found in Japanese patients (Tsukamoto et al., 2003) and analyzed the localization and anion transporter activity of these mutant proteins *in vitro* and the effects of salicylate as a pharmacological chaperone for the rescue of the pendrin mutants.

2. Methods

2.1. Construction of expression vectors

The sequences encoding an N-terminal FLAG tag were added by PCR amplification to the cDNA for human wild-type pendrin (Accession No. NM_000441.1) and the resulting insert was cloned into pcDNA3.1 (Invitrogen, Carlsbad, CA). *E. coli* JM109 was transformed with the constructed expression vector (pcDNA3.1/pendrin-FLAG). Mutational studies targeted the genes of pendrin missense mutations reported in Japanese patients (Tsukamoto et al., 2003). To express 10 pendrin mutants, the mutations were introduced into the pcDNA3.1/pendrin-FLAG using the primer sets shown in Table 1 and QuikChange II Site-Directed Mutagenesis Kit (Stratagene, La Jolla, CA) according to the manufacturer's protocol. The constructs were verified by DNA sequence analysis.

2.2. Cell culture

HEK293 cells (RIKEN Cell Bank, Tsukuba, Japan) were maintained in RPMI-1640 medium (Sigma, St. Louis, MO) supplemented with 10% fetal bovine serum (FBS) at 37 °C in a humidified atmosphere of 5% CO2. For the experiments, HEK293 cells were seeded in each well of 6-well plate at a density of 5×10^5 cells in 2 ml of 10% FBS-RPMI-1640 medium. After 12 h, each expression vector (2 μg) was transfected into HEK293 cells using FuGENE HD Transfection

Table 1
The sequences of primer sets for site-directed mutagenesis.

Primers	Sequences	
p.P123S	Forward	5′ GGATATGGTCTCTACTCTGCTTTTTTCTCCATCCTGACAT AC 3′
	Reverse	5′ GTATGTCAGGATGGAGAAAAAAGCAGAGTAGAGACCATATCC 3′
p.M147V	Forward	5′ CTTTTCCAGTGGTGAGTTTAGTGGTGGGATCTGTTGTTC 3′
	Reverse	5′ GAACAACAGATCCCACCACTAAACTCACCACTGGAAAAG 3′
p.K369E	Forward	5′ CTATTGCAGTGTCAGTAGGAGAAGTATATGCCACCAAGTATG 3′
	Reverse	5′ CATACTTGGTGGCATATACTTCTCCTACTGACACTGCAATAG 3′
p.A372V	Forward	5′ GTGTCAGTAGGAAAAGTATATGTCACCAAGTATGATTACACC 3′
	Reverse	5′ GGTGTAATCATACTTGGTGACATATACTTTTCCTACTGACAC 3′
p.N392Y	Forward	5′ GCCTTTGGGATCAGCTACATCTTCTCAGGATTCTTC 3′
	Reverse	5′ GAAGAATCCTGAGAAGATGTAGCTGATCCCAAAGGC 3′
p.C565Y	Forward	5′ CGATGGTTTTAAAAAATATATCAAGTCCACAGTTGGATTTGATGCC 3′
	Reverse	5′ GGCATCAAATCCAACTGTGGACTTGATATATTTTTTAAAACCATCG 3′
p.S657N	Forward	5′ CAAAGTGCCAATCCATAACCTTGTGCTTGACTGTG 3′
	Reverse	5′ CACAGTCAAGCACAAGGTTATGGATTGGCACTTTG 3′
p.S666F	Forward	5′ CTTGACTGTGGAGCTATATTTTTCCTGGACGTTGTTG 3′
	Reverse	5′ CAACAACGTCCAGGAAAAATATAGCTCCACAGTCAAG 3′
p.T721M	Forward	5′ CAACATTAGAAAGGACACATTCTTTTTGATGGTCCATGATGC 3′
	Reverse	5′ GCATCATGGACCATCAAAAAGAATGTGTCCTTTCTAATGTTG 3′
p.H723R	Forward	5′ CTTTTTGACGGTCCGTGATGCTATACTCTATCTACAG 3′
	Reverse	5′ C TGTAGATAGAGTATAGCATCACGGACCGTCAAAAAG 3′

Reagent (Roche, Grenzacherstrasse, Switzerland) according to the manufacturer's protocol. After transfection for 24–48 h, the cells were used for the following experiments.

2.3. Immunofluorescence microscopy

After incubation for 24 h of HEK293 cells transfected with each vector, the cells were replaced in 24-well glass bottom plates and further incubated for 24 h. Salicylate dissolved in distilled water was added to the cells in each well and the cells were incubated for 12 h in the presence of salicylate. For vehicle control, distilled water was added to the medium. The cells were washed 3 times with PBS and fixed with 4% paraformaldehyde for 5 min at room temperature. To avoid non-specific binding, the cells were incubated in blocking solution (50% Block Ace, Dainippon Sumitomo Pharma, Osaka, Japan and 50% FBS) for 1 h at 37 °C. After washing with PBS, the cells were incubated with mouse anti-FLAG primary antibody (Sigma) for 1 h at 37 °C and then anti-mouse IgG secondary antibody TRITC conjugated (Sigma) for 30 min at 37 °C. These antibodies were diluted in 0.1% (w/v) saponin-PBS. After washing with PBS, the fluorescence of cells stained with TRITC was observed using a confocal laser scanning microscope (FV500, Olympus, Tokyo, Japan).

To clarify where pendrin mutants are mainly expressed in the cells, fluorescence intensities of the cells were analyzed by FLUOVIEW (Olympus). As shown in Fig. 1, a green line was firstly drawn on the cell expressing wild-type pendrin, and intensities of TRITC and differential interference contrast (DIC) on the line were analyzed. Two peaks at the ends of the line in the TRITC intensity map and two low peaks in the DIC intensity map were detected. The two low peaks in the DIC intensity map showed the border between the cell and the glass of the culture plate. The width of the plasma membrane was determined to be 0.8 μm from the border, based on the width of the TRITC-related peaks in the TRITC intensity map. Then, the fluorescence intensities were obtained from the 20 regions (region size, 0.8 μm × 0.8 μm) of the plasma membrane area, and such intensities were also obtained from the 20 regions of the cytoplasm area. Each region was not overlapped and equally distributed from the cell center. The former and the latter regions covered approximately 90% and 70% of the plasma membrane area and the cytoplasm area, respectively. The ratio of the mean fluorescence intensities of the 20 regions obtained from the plasma membrane area to such intensities of the 20 regions obtained from the cytoplasm area was calculated. Finally, the main localization of each pendrin mutant was estimated by calculating the averaged ratio from the ratio obtained from 6 to 9 cells.

2.4. Iodide efflux assay

Iodide efflux from cells was assessed by a modification of the methods described by Gillam et al. (2004) and Dossena et al. (2006). After incubation for 36 h of HEK293 cells transfected with each vector, the cells in each well of the 6-well plate were incubated for 12 h at 37 °C in the medium in the presence or absence of salicylate. The cells were then incubated for 10 min at 37 °C in 1 ml of high Cl^- buffer (2 mM KCl, 135 mM NaCl, 1 mM CaCl2, 1 mM MgCl2, 10 mM D-glucose, 20 mM HEPES, pH7.4), and further incubated for 60 min at 37 °C in 1 ml of high I^- buffer (2 mM KCl, 135 mM NaI, 1 mM CaCl2, 1 mM MgCl2, 10 mM D-glucose, 20 mM HEPES, pH7.4) containing 200 kBq/ml ^{125}I. During these processes, uptake of ^{125}I is promoted by exchange with Cl^- already taken into the cells by a mechanism independent of pendrin. After washing with high I^- buffer, the cells were incubated for 10 min at 37 °C in 1 ml of high Cl^- buffer.

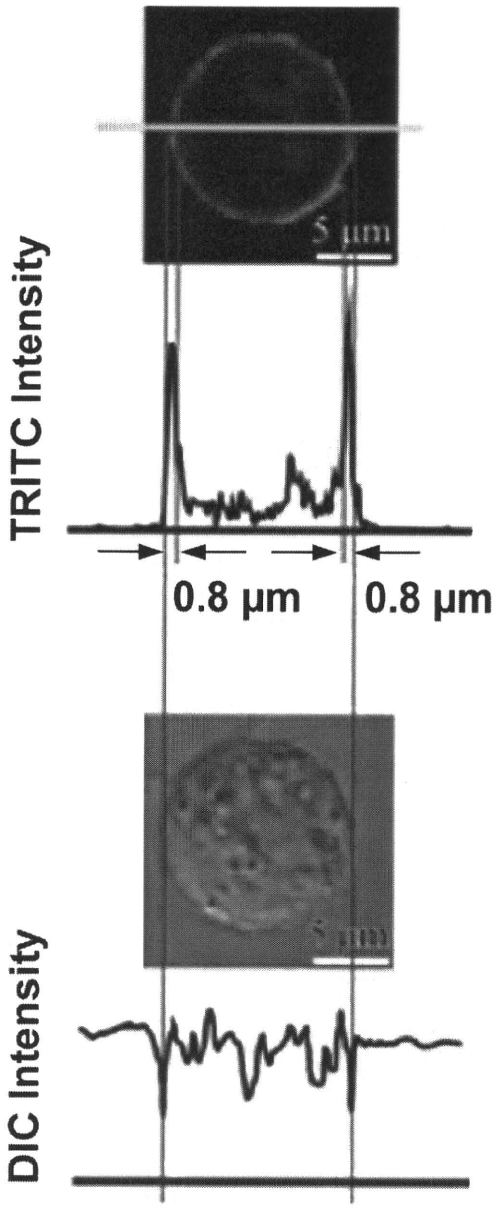

Fig. 1. Intensity analysis of intracellular localization of pendrin. A green line was drawn on the cell expressing wild-type pendrin, which mainly expresses in plasma membrane, and the intensities of TRITC and DIC on the line were analyzed. Two peaks at the ends of the line in the TRITC intensity map and the two low peaks in the DIC intensity map were detected. The two low peaks in the DIC intensity map showed the border between the cell and glass of the culture plate. The width of plasma membrane was determined to be 0.8 μm based on width of the TRITC-related peaks in the TRITC intensity map, and 0.8 μm inside from the border was defined the plasma membrane. (For interpretation of the references to colour in this figure legend, the reader is referred to the web version of this article.)

Replacement of high I^- buffer by high Cl^- buffer induces the export of ^{125}I from within cells to extracellular media by the activity of transfected pendrin. Finally, the cells were lysed in 200 μl of lysis buffer (0.1 M NaOH, 0.1% SDS, 2% sodium carbonate), and intracellular iodide content was determined by measuring radiolabeled-iodide in the cell lysates using a scintillation counter. The protein content in the lysates was measured by Bradford methods (Bio-Rad, Hercules, CA). Remaining radioactivity in cells was obtained by dividing intracellular iodide content in the lysates (cpm/ml) by protein content in the lysates (mg/ml).

2.5. Cytotoxicity assay

HEK293 cells cultured in each well of a 24-well glass bottom plate were incubated for 12 h at 37 °C in medium in the presence or absence (vehicle control) of 10 mM of salicylate. After incubation, nuclei in the cells were stained with 7-amino-actinomycin D (7-AAD, 200 ng/ml in medium) (Sigma) at 37 °C for 10 min. As 7-AAD penetrates plasma membranes of dying or dead cells but not viable cells, this compound is used as a marker for cell death. As a positive control, the plasma membrane of cells was permeated by incubation in methanol for 1 min and dried prior to the staining with 7-AAD. The fluorescence of the cells was observed by a confocal laser scanning microscope (Olympus).

2.6. Statistical analysis

The statistical significance of the results was analyzed using Dunnett's test for multiple comparisons and Student's *t*-test for unpaired observations.

3. Results

3.1. Expression of pendrin mutants in HEK293 cells

When wild-type pendrin was expressed in HEK293 cells, the fluorescence intensity of TRITC, which indicates localization of pendrin, was particularly strong on the plasma membrane compared with the fluorescence intensity of the empty vector transfected cells (Fig. 2). Two pendrin mutants, i.e., p.K369E and p.C565Y, were also localized on the plasma membrane (Fig. 2). On the other hand, other mutants, i.e., p.P123S, p.M147V, p.A372V, p.N392Y, p.S657N, p.S666F, p.T721M and p.H723R, were localized in the whole cell except for the regions of the nuclei (Fig. 2). These findings indicate that wild-type pendrin and two pendrin mutants, p.K369E and p.C565Y, were localized in the plasma membrane, whereas the other 8 pendrin mutants were retained in the cytoplasm.

3.2. Effects of salicylate on the localization of mutant pendrin

Eight pendrin mutants, i.e., p.P123S, p.M147V, p.A372V, p.N392Y, p.S657N, p.S666F, p.T721M and p.H723R, were retained in the cytoplasm of the HEK293 cells (Fig. 2). Therefore, we analyzed whether these 8 pendrin mutants are induced normal transport to the plasma membrane by salicylate. The 8 pendrin mutants were localized in cytoplasm when the cells were incubated in the absence of salicylate (Fig. 3a and c). In contrast, 10 mM of salicylate made the fluorescence intensity of TRITC of the plasma membrane stronger than that of the cytoplasm in the cells which expressed p.P123S, p.M147V, p.S657N and p.H723R (Fig. 3b and c). In this case, the fluorescence intensity of cytoplasm by TRITC becomes weaker and the nucleus and cytoplasm in the cell become unclear, because the pendrin mutants, i.e., p.P123S, p.M147V, p.S657N and p,H723R, translocate by the compound from the cytoplasm to the plasma membrane (Fig. 3b and c). As a result, the nucleus appears to be large (Fig. 3b). However, no changes were observed in the cells transfected with other mutants, i.e., p.A372V, p.N392Y, p.S666F and p.T721M (Fig. 3b and c). These findings indicate that salicylate induces the translocation of p.P123S, p.M147V, p.S657N and p.H723R pendrin mutants from the cytoplasm to the plasma membrane.

3.3. Effect of salicylate on the viability of HEK293 cells

To clarify whether 10 mM of salicylate has cytotoxicity, HEK293 cells were incubated for 12 h at 37 °C with or without 10 mM of salicylate, and the viability of cells was visualized by microscope. On treatment with salicylate, as well as vehicle control, no significant fluorescence intensity of 7-AAD binding to nuclei in the cells was observed (Fig. 4). In contrast, as a positive control, nuclei of the cells treated with methanol were clearly stained due to the increase in the permeability of the plasma membrane (Fig. 4). These findings indicate that 10 mM of salicylate has no cytotoxicity to HEK293 cells.

3.4. Effects of lower concentration of salicylate on the intracellular localization of p.P123S mutant pendrin

HEK293 cells expressing p.P123S pendrin mutant were incubated for 12 h in medium containing 1 or 10 mM of salicylate. The intracellular localization of the p.P123S pendrin mutant was detected by immunofluorescence microscopy. The p.P123S pendrin mutant was localized in plasma membrane when the cells were incubated in the presence of 10 mM of salicylate (Fig. 5). However, 1 mM of salicylate did not change the localization of p.P123S pendrin mutant when compared with vehicle control (Fig. 5). These findings indicate that salicylate at 10 mM but not at 1 mM induces the translocation of p.P123S mutant pendrin.

3.5. Effects of salicylate on the activity of pendrin

We analyzed whether the 4 pendrin mutants (p.P123S, p.M147V, p.S657N and p.H723R) translocated to the plasma membrane by salicylate act as transporters using radiolabeled-iodide. HEK293 cells transfected with the expression vector for the pendrin mutants were incubated with or without salicylate. In cells transfected with the wild-type pendrin expression vector, remaining radioactivity in cells was significantly decreased compared with that transfected with an empty vector when the cells were incubated in the absence of salicylate (Fig. 6). This finding indicates that wild-type pendrin has an activity to export iodide from cytoplasm. Remaining radioactivity in cells expressing the p.K369E or p.C565Y mutants, which were located in the plasma membrane as shown in Fig. 1, was decreased as in the case of wild-type pendrin (Fig. 6). Therefore, the mutants acted to transport iodide as do wild-type pendrin. In the expression of wild-type pendrin, the activity in the presence of 10 mM of salicylate was not significantly different from that in the absence of salicylate (Fig. 6), suggesting that the incubation with of 10 mM of salicylate does not affect the cellular condition and the wild-type pendrin activity. In case of transfection with 4 mutant pendrin genes encoding the mutants p.P123S, p.M147V, p.S657N and p.H723R, no significant change of remaining radioactivity in cells was observed compared with the empty control in the absence of salicylate treatment (Fig. 6). However, the remaining radioactivity in cells transfected with each mutant was significantly decreased by 10 mM of salicylate treatment (Fig. 6). These activities were almost the same as in the case of wild-type pendrin (Fig. 6). These findings indicate that salicylate restores pendrin activity.

4. Discussion

It is suggested that retention of some pendrin mutants in the endoplasmic reticulum is a major mechanism for Pendred syndrome (Rotman-Pikielny et al., 2002; Dossena et al., 2009). p.L236P, p.G384 and p.T416P pendrin mutants reported in Caucasians are accumulated in the endoplasmic reticulum and do not reach the plasma membrane due to their mutations (Rotman-Pikielny et al., 2002). In Japanese patients, 10 pendrin mutants, i.e., p.P123S, p.M147V, p.K369E, p.A372V, p.N392Y, p.C565Y, p.S657N, p.S666F, p.T721M and p.H723R, have been reported (Tsukamoto et al., 2003). Yoon et al. (2008) have reported that p.M147V and p.H723R pendrin mutants were accumulated in the endoplasmic reticulum due to their mutation. However,

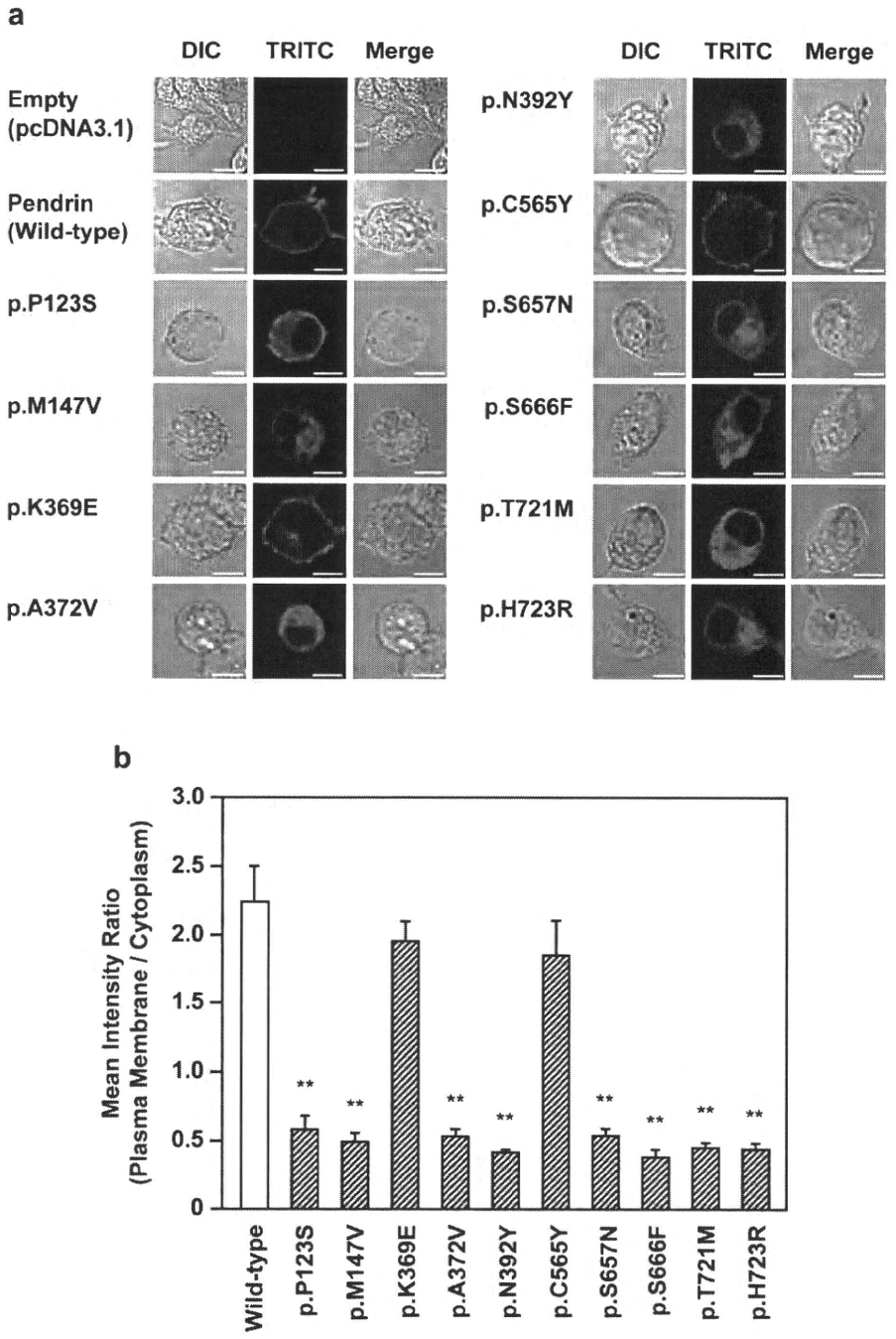

Fig. 2. Intracellular localization of pendrin and its mutants in HEK293 cells. HEK293 cells were transfected with the empty vector, the expression vector including wild-type pendrin gene or the mutant genes. (a) After 48 h, intracellular localization of pendrin was analyzed by immunofluorescent staining. The experiment shown is representative of 3 independent experiments. (b) The fluorescence intensities of the plasma membrane and cytoplasm of the cells were evaluated. The ratios were obtained by calculating the mean fluorescence intensities of 20 regions (0.8 μm × 0.8 μm) in plasma membrane and cytoplasm. Values are the means from 6 to 9 cells with SEM. $^{**}P < 0.01$ vs. wild-type. This figure shows that wild-type pendrin and two pendrin mutants p.K369E and p.C565Y were localized in the plasma membrane, whereas the other 8 pendrin mutants were retained in the cytoplasm. The bar indicates 10 μm.

intracellular localization and activity of 8 other pendrin mutants have remained to be elucidated. In this study, we demonstrated the following 4 points about the intracellular localization and activity of pendrin mutants reported in Japanese patients: (1) Among the 10 pendrin mutants reported in Japanese patients, p.K369E and p.C565Y are expressed in the plasma membrane of HEK293 cells, as is wild-type pendrin. (2) The other 8 mutants, i.e., p.P123S, p.M147V, p.A372V, p.N392Y, p.S657N, p.S666F, p.T721M and p.H723R, are accumulated in the cytoplasm of the cells. (3) In the 8 pendrin mutants retained in the cytoplasm of the cells, p.P123S, p.M147V, p.S657N and p.H723R are induced normal transport to the plasma membrane of the cells by 10 mM salicylate without cytotoxicity. (4) When induced normal transport to the plasma membrane by salicylate, these 4 pendrin mutants recovered their activity.

Pendrin is a member of the *SLC26A* gene family including prestin (Mount and Romero, 2004). In the inner ear, it is reported that the motor protein prestin plays an important role in hearing as the

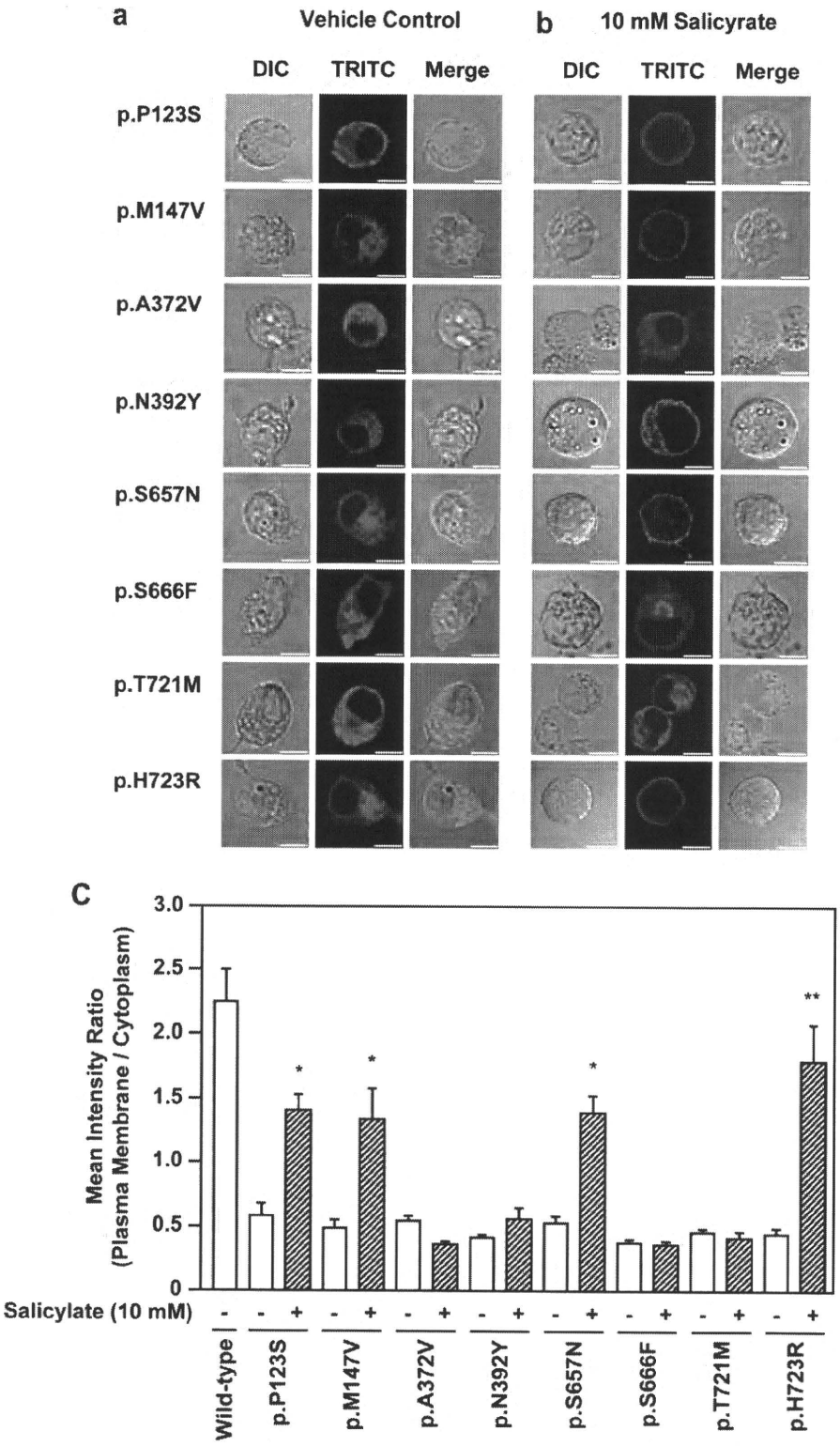

Fig. 3. Effects of salicylate on the intracellular localization of mutant pendrin. HEK293 cells were transfected with the expression vector including mutant pendrin gene. After 36 h, salicylate was added to the medium and the cells were further incubated for 12 h (a, b) Intracellular localization of pendrin was analyzed by immunofluorescent staining. The experiment shown is representative of 3 independent experiments. (c) The fluorescence intensities of the plasma membrane and cytoplasm of the cells were evaluated. The ratios were obtained by calculating the mean fluorescence intensities of 20 regions (0.8 μm × 0.8 μm) in plasma membrane and cytoplasm. Values are the means from 6 to 9 cells with SEM. $^{*}P < 0.05$, $^{**}P < 0.01$ vs. wild-type. This figure reveals that after incubation with salicylate, fluorescence intensity of TRITC of plasma membrane is stronger than that of the cytoplasm in the cells expressing p.P123S, p.M147V, p.S657N and p.H723R, but not in those expressing p.A372V, p.N392Y, p.S666F and p.T721M. The bar indicates 10 μm.